Astrometry and Photometry for ≈1000 L, T, and Y Dwarfs from the UKIRT Hemisphere Survey

Adam C. Schneider[1] , Jeffrey A. Munn[1] , Frederick J. Vrba[1], Justice Bruursema[1] , Scott E. Dahm[2] , Stephen J. Williams[1], Michael C. Liu[3] , and Bryan N. Dorland[4]

[1] United States Naval Observatory, Flagstaff Station, 10391 West Naval Observatory Road, Flagstaff, AZ 86005, USA; adam.c.schneider4.civ@us.navy.mil
[2] Gemini Observatory/NSF's NOIRLab, 950 North Cherry Avenue, Tucson, AZ 85719, USA
[3] Institute for Astronomy, University of Hawaii at Manoa, Honolulu, HI 96822, USA
[4] United States Naval Observatory, 3450 Massachusetts Avenue Northwest, Washington, DC 20392-5420, USA
Received 2023 June 16; revised 2023 July 19; accepted 2023 July 20; published 2023 August 14

Abstract

We present the positions, proper motions, and near-infrared photometry for 966 known objects with spectral types later than M that were observed as part of the the UKIRT Hemisphere Survey (UHS). We augment the photometry and astrometry from UHS with information from Gaia DR3, Pan-STARRS DR2, and CatWISE 2020 to produce a database of homogeneous photometry and astrometry for this sample. The multi-epoch survey strategy of UHS allows us to determine the proper motions for most sources, with a median proper motion uncertainty of ∼3.6 mas yr^{-1}. Our UHS proper motion measurements are generally in good agreement with those from Gaia DR3, Pan-STARRS, and CatWISE 2020, with UHS proper motions typically more precise than those from CatWISE 2020 and Pan-STARRS but not Gaia DR3. We critically analyze the publicly available spectra for 406 members of this sample and provide updated near-infrared spectral types for ∼100 objects. We determine typical colors as a function of spectral type and provide absolute magnitude versus spectral type relations for UHS *J*- and *K*-band photometry. Using newly determined proper motions, we highlight several objects of interest, such as objects with large tangential velocities, widely separated co-moving companions, and potential members of young nearby associations.

Unified Astronomy Thesaurus concepts: Brown dwarfs (185); L dwarfs (894); T dwarfs (1679); Y dwarfs (1827); Low mass stars (2050)

Supporting material: machine-readable table

1. Introduction

Large-scale optical and infrared surveys, such as Deep Near-Infrared Southern Sky Survey (DENIS; Epchtein et al. 1997), the Sloan Digital Sky Survey (SDSS; York et al. 2000), the Two Micron All-Sky Survey (2MASS; Skrutskie et al. 2006), the Wide-field Infrared Survey Explorer (WISE; Wright et al. 2010), and the Panoramic Survey Telescope And Rapid Response System (Pan-STARRS; Kaiser et al. 2010), have been instrumental in the discovery and characterization of the vast majority of the known ultracool population. These efforts, combined with dedicated spectroscopic follow-up campaigns, have led to the definition of the L, T, and Y spectral classes (e.g., Kirkpatrick 2005; Cushing et al. 2011), as well as subpopulations within these classes, such as low-metallicity subdwarfs (e.g., Burgasser et al. 2003a; Zhang et al. 2017) and young low-gravity substellar objects (e.g., Kirkpatrick et al. 2008; Allers & Liu 2013; Faherty et al. 2016).

Large homogeneous samples of brown dwarfs have been valuable for characterizing the known population, as well as analyzing individual objects (e.g., Kirkpatrick et al. 2011; Best et al. 2018). The UKIRT Hemisphere Survey (UHS) covers approximately 12,700 deg² of the northern hemisphere with near-infrared *J* and *K* filters between 0° and 60° (Dye et al. 2018; J. Bruursema et al. 2023, in preparation). We have

gathered photometric and astrometric information for all known L, T, and Y dwarfs within the UHS footprint, using both the previously released *J*-band portion of the survey (DR1; Dye et al. 2018) and the newly released *K*-band UHS data (DR2; J. Bruursema et al. 2023, in preparation). The creation of the sample is described in Section 2. We describe the photometry of the sample in Section 3 and describe new proper motion measurements in Section 4. In Section 5, we describe efforts to identify new young moving group members, objects with large tangential velocities, and co-moving companions among this sample. We summarize our results in Section 6.

2. Sample Selection

The goal of this work is to compile UHS astrometry and photometry for known L, T, and Y dwarfs in the UHS footprint. We select only those objects with spectroscopically determined spectral types (i.e., no photometric brown dwarf candidates). Our initial list of candidates for the creation of this sample was the UltracoolSheet,[5] a public compilation of ultracool dwarfs (e.g., spectral types later than ∼M6) and directly imaged exoplanets compiled in Best et al. (2020). To this list, we added several papers with spectroscopically classified L, T, or Y dwarfs that were either not included (Robert et al. 2016; Kellogg et al. 2017; Kuchner et al. 2017; Pérez-Garrido et al. 2017, 2018; Schneider et al. 2017; Greco et al. 2019; Kiman et al. 2019; Zhang et al. 2019) or published after the creation of the UltracoolSheet in 2020 (Faherty et al. 2020, 2021;

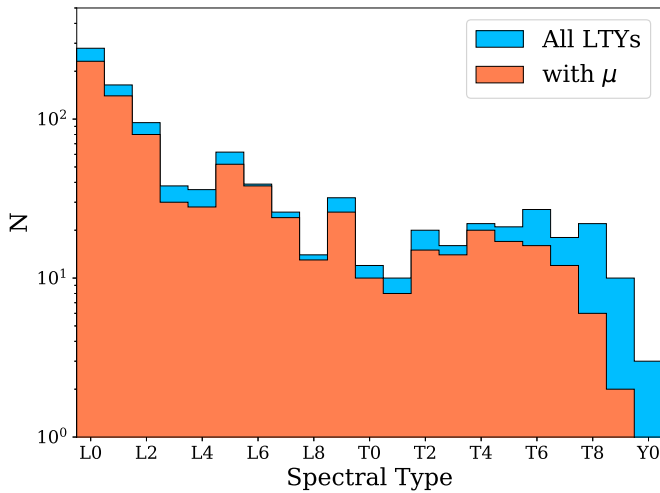---

[5] http://bit.ly/UltracoolSheet

Figure 1. Histogram of spectral types for the sample of known L, T, and Y dwarfs in the UHS catalog. Note the logarithmic y-scale. The orange histogram shows the subset of objects from the sample that have newly measured proper motions in this work. The entire sample contains 966 L, T, and Y dwarfs, of which 782 have newly measured proper motions using UHS data.

Meisner et al. 2020b, 2021; Schneider et al. 2020, 2022; Zhang et al. 2020; Marocco et al. 2021; Kirkpatrick et al. 2021; Kiwy et al. 2022; Softich et al. 2022; Vos et al. 2022).

Because L, T, and Y dwarfs can have large proper motions, we first performed a cross-match with a large search radius (1′) to determine which objects from this initial list were likely covered by the UHS survey. We then individually checked for detections of each object using UHS images and previously measured positions. A total of 966 L, T, and Y dwarfs were found to have at least one detection in UHS DR2. Figure 1 shows a histogram of the spectral types of this sample (see Section 2.2). As seen in the figure, a significant portion of this sample consists of early L dwarfs from various Sloan Digital Sky Survey (SDSS) surveys (West et al. 2008; Schmidt et al. 2010; West et al. 2011; Kiman et al. 2019), though every spectral type bin earlier than Y0 has $\geqslant$10 objects. The histogram also shows the portion of the entire sample for which new proper motion measurements were calculated using UHS data ($\sim$81% of all objects), which will be discussed further in Section 4.

The positions, and UHS J- and K-band photometry for objects in this sample pulled directly from UHS DR2 (J. Bruursema et al. 2023, in preparation) are given in Table A1. We also include J- and K-band positions, uncertainties, and epochs for each object after re-registering to the Gaia DR3 (Gaia Collaboration et al. 2023) reference frame (see Section 4).

2.1. Additional Photometry and Astrometry

We include photometry and astrometry from Gaia DR3 (Gaia Collaboration et al. 2023), Pan-STARRS DR2 (Chambers et al. 2016; Magnier et al. 2020), and CatWISE 2020 (Marocco et al. 2021) for each object, when available. These data allow us to evaluate our derived proper motions and to compile more complete spectral energy distributions to determine color trends with spectral type utilizing UHS photometry. Relevant photometry and astrometric measurements from these surveys are given in Table A1.

Table 1
Updated Near-infrared Spectral Types

Name	Prev. NIR Type	References	New Type
WISEA J000627.85+185728.8	L7	1	L6 (sl. red)
2MASSW J0015447+351603	L1	2	L2
2MASS J00282091+2249050	L5	3	L6
2MASSW J0030438+313932	L3.2	2	L2
2MASSW J0228110+253738	L0	6	L1
SDSS J024256.98+212319.6	L4	7	L5.5
2MASS J03250136+2253039	L3.3	2	L2
2MASSJ03440892+0111251	L2.9:	2	L1 (sl. blue)
2MASS J07244848+2506143	L4	9	L3
2MASSW J0740096+321203	L4	2	L5
SDSS J080048.13+465825.5	L1.3	2	L0.5
SDSS J081253.19+372104.2	L0.5 pec	10	M9 (sl. red)
SDSS J081757.49+182405.0	L2	2	L0.5
SDSS J084333.28+102443.5	L2.7:	2	L1 (sl. blue)
SDSS J092308.70+234013.7	L2.3	2	L1 (sl. blue)
2MASS J09325053+1836485	L6	9	L4.5
SDSS J094047.88+294653.0	L2:	10	L1
2MASS J09481259+5300387	L2	9	L1
2MASS J10271549+5445175[a]	L7	9	L2 VL-G
SDSS J103321.92+400549.5	L6	7	L5 (blue)
SDSS J111320.16+343057.9	L3	7	L2
2MASS J12312141+4959234	L3.4	2	L2
2MASS J12352675+4124310	L5	9	L2: (red)
2MASS J12453705+4028456	L1	9	L2 (blue)
2MASSW J1246467+402715	L4	2	L5
2MASSI J1305410+204639	L6.5	2	L5
2MASS J13451417+4757231	L3	9	L5.5
SDSS J142612.86+313039.4	L4::	2	L5
SDSS J143832.63+572216.9	L4.6	2	L3.5
SDSS J152039.82+354619.8	T0 $\pm$ 1	7	L9
2MASS J15311344+1641282	L1	12	L2
SDSS J154849.02+172235.4	L5	7	L8.5
2MASS J15500191+4500451	L6	9	L2 (red)
SDSS J155120.86+432930.3	L3.1	2	L2
2MASS J15543602+2724487	L5	9	L6
2MASS J16094569+1426422	L4	9	L2
SDSS J161459.98+400435.1	L2	13	L3
SIMP J16270845+0546304	L0	10	M9
2MASS J16304139+0938446	L0.4:	2	L1.5
2MASS J17120142+3108217	L3	9	L2
2MASS J17161258+4125143	L4	14	L2
2MASSI J1721039+334415	L5.3:	2	L3 (blue)
LSPM J1731+2721	L0	15	M9
WISE J173332.50+314458.3	L2	13	L3.5 (red)
WISEA J174336.62+154901.3	L1 pec (blue)	8	M9.5
2MASSI J2057153+171515	M9.9	2	L1 (sl. red)
SDSS J214046.55+011259.7	L4.5	3	L2 (sl. blue)
PSO J344.8146+20.1917	L2.5	16	L4 (sl. red)

Note.
[a] See text in Section 2 for a discussion of this object.

References. (1) Schneider et al. (2016); (2) Bardalez Gagliuffi et al. (2014); (3) Burgasser et al. (2010); (4) Burgasser et al. (2004); (5) Kirkpatrick et al. (2011); (6) Wilson et al. (2003); (7) Chiu et al. (2006); (8) Luhman & Sheppard (2014); (9) Kellogg et al. (2017); (10) Robert et al. (2016); (11) Sheppard & Cushing (2009); (12) Faherty et al. (2009); (13) Thompson et al. (2013); (14) Kellogg et al. (2015); (15) Allers & Liu (2013); (16) Best et al. (2015).

Table 2
New Near-infrared Spectral Types

Name	Opt. Type	References	NIR Type
2MASSI J0025036+475919	L4:	1	L3.5 (red)
2MASSI J0213288+444445	L1.5	2	L0.5
SDSS J080027.57+551134.1	L1	3	L1
2MASSI J1117369+360936	L0?	2	L1
SDSS J134148.85+551046.2	L2	4	L3
SDSS J153012.87+514717.1	L0	5	M9
SDSS J161611.36+521328.0	L0	5	L0
SDSS J163437.19+233620.5	L1	4	L1
2MASSW J1841086+311727	L4 pec	6	L5
2MASS J21522609+0937575	L7:	7	L7
2MASS J22490917+3205489	L5	1	L5 (red)

References. (1) Cruz et al. (2007); (2) Cruz et al. (2003); (3) Schmidt et al. (2010); (4) Kiman et al. (2019); (5) West et al. (2008); (6) Kirkpatrick et al. (2000); (7) Cruz et al. (2018).

2.2. Spectral Types

Spectral types were taken from the literature for most objects, with exceptions detailed in the following paragraphs. For objects with multiple spectral type determinations, we use the first measured type if all measurements agree, and preferentially use the most recent measurements when disagreements arise. We list optical and near-infrared spectral types for this sample in Table A1.

In an effort to have consistent spectral types, we searched for existing IRTF/SpeX near-infrared spectroscopy in the SpeX Prism Library Analysis Toolkit (SPLAT; Burgasser & Splat Development Team 2017) for every object in this sample to confirm or refine spectral types. In total, 406 objects were found to have near-infrared spectra in the SPLAT archive. To derive near-infrared spectral types, we compared each spectrum to the T dwarf spectral standards in Burgasser et al. (2006a) and the L dwarf spectral standards of Kirkpatrick et al. (2010), with the exception that we use 2MASSI J0825196+211552 as the L7 standard, as recommended in Cruz et al. (2018). We also use the subdwarf standards defined in Greco et al. (2019) when appropriate. Using such existing spectra, we generally find good agreement with previously determined spectral types to within 0.5 subtypes. We found 48 objects with previously determined near-infrared spectral types that differ by a full subtype or more from our determination, which are listed in Table 1.

In this work, we prefer near-infrared spectral types over optical spectral types because of the infrared nature of the UHS survey. Thus, for objects with only optical types in the literature, we again searched the SPLAT database to update to near-infrared types when possible. New near-infrared types were found for 11 objects with existing optical spectral types and are listed in Table 2. One object, (SDSS J153012.87 +514717.1) is typed as L0 in the optical (West et al. 2008) but M9 in the near-infrared, and is thus excluded from the final sample.

2.3. Notes on Object Spectral Types

2.3.1. 2MASS J10271549+5445175

2MASS J10271549+5445175 was discovered in Kellogg et al. (2017) and assigned a spectral type of L7. Our reanalysis
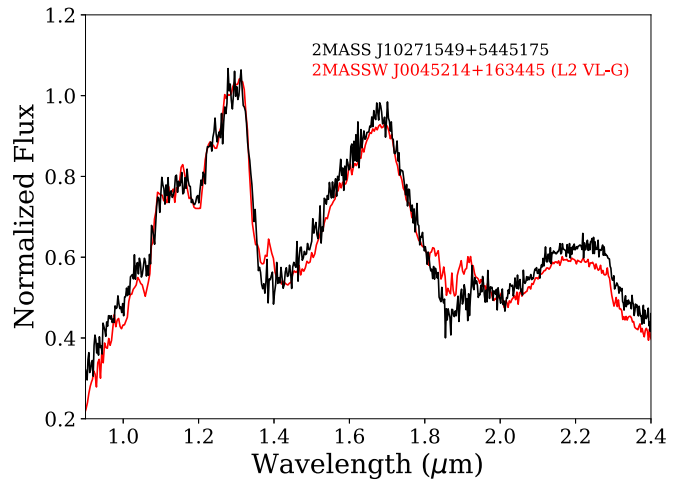

Figure 2. The near-infrared spectrum of 2MASS J10271549+5445175 compared to the L2 VL-G object 2MASSW J0045214+163445. Each spectrum is normalized to the J-band peak between 1.27 and 1.29 μm.

using the available spectrum in SPLAT instead found that this object is likely to be a low-gravity early-type L dwarf. Figure 2 shows a comparison of the near-infrared spectrum of this object to 2MASSW J0045214+163445, which is typed as L2 VL-G in Allers & Liu (2013) and L2γ in Faherty et al. (2016). We find that the spectrum of 2MASS J10271549+5445175 is an excellent match to that of 2MASSW J0045214+163445, and we therefore assign this object a spectral type of L2 VL-G (or L2γ). This classification is bolstered by the low-gravity indices defined in Allers & Liu (2013) applicable to the low-resolution spectrum—we find FeH$_z$, VO$_z$, K I$_J$, and H-cont values of 1.052, 1.079, 0.988, and 0.989, respectively, which leads to a gravity score of 2022 (i.e., VL-G). This object is discussed further in Section 5.1.2.

2.3.2. Newly Classified Subdwarfs

The near-infrared spectra of several objects showed hallmarks of being low-metallicity subdwarfs, such as suppressed emission in the H- and K-bands due to enhanced collisionally-induced H$_2$ absorption (see e.g., Zhang et al. 2017). To classify these objects, we compared their spectra to the near-infrared subdwarf standards suggested in Greco et al. (2019). Since there is no sdL0 standard in Greco et al. (2019), we propose the subdwarf SSSPM J1444−2019 (Scholz et al. 2004) as the sdL0 near-infrared standard because it is classified as an sdL0 in the optical and near-infrared in Kirkpatrick et al. (2016). Another object, 2MASS J00412179+3547133, was given a near-infrared classification of sdL? in Burgasser et al. (2004) and classified in the optical as sdL0.5 (Zhang et al. 2017). The spectrum of this object is intermediate between our sdL0 standard (SSSPM J1444−2019) and the sdL1 standard (2MASS J17561080+2815238; Kirkpatrick et al. 2010). We therefore suggest 2MASS J00412179+3547133 as the sdL0.5 near-infrared template.

Objects with new or updated spectral types that place them in the sdL class are listed in Table 3 and shown in Figure 3. Note that three objects (SDSS J112647.03+581632.2, 2MASSW J1300425+191235, and SDSS J165850.26 +182000.6) are classified as d/sdL1 and are compared to the sdL1 and L1 spectral standards in the figure. Several of these

Table 3
Newly Classified Subdwarfs

Name	Prev. NIR Type	References	New Type
2MASS J00412179+3547133[a]	sdL?	1	sdL0.5
WISEA J030845.36+325923.1	L1 pec (blue)	2	sdL1
SDSS J075054.74+445418.7	M8 pec	3	sdL0.5
SDSS J112647.03+581632.2	L1.3	4	d/sdL1
2MASSW J1300425+191235	L1.7	4	d/sdL1
2MASS J14313097+1436539	L2	5	sdL1
2MASS J14343616+2202463	sdM9	5	sdL1
SDSS J145255.58+272324.4	L0.2:	4	sdL1
2MASS J16403197+1231068	sdM8?	1	sdL0:
SDSS J165850.26+182000.6	L0.9	4	d/sdL1

Note.
[a] Classified as sdL0.5 in the optical by Zhang et al. (2017) and suggested in this work as the sdL0.5 near-infrared template.
References. (1) Burgasser et al. (2004); (2) Luhman & Sheppard (2014); (3) Thompson et al. (2013); (4) Bardalez Gagliuffi et al. (2014); (5) Sheppard & Cushing (2009).

objects have kinematics consistent with membership in the old thick-disk population, and are discussed further in Section 5.2.

3. Photometry

The photometry from the UHS survey is based on the UKIRT photometric system (Hodgkin et al. 2009), which was designed to closely match photometry from the Mauna Kea Observatories (MKO) system (Simons & Tokunaga 2002). The J- and K-band photometry for all known L, T, and Y dwarfs detected in the UHS survey are taken directly from UHS DR2 and are given in Table A1.

This photometry can be used to find typical UHS colors and absolute magnitudes for the various spectral types included in this sample. There are many factors that determine a specific L, T, or Y dwarf color, most notably effective temperature (T_{eff}) but also surface gravity (e.g., Allers & Liu 2013), inclination angle (e.g., Vos et al. 2017), unresolved binarity (e.g., Burgasser et al. 2010), and cloud composition (e.g., Hiranaka et al. 2016). These properties can lead to objects having colors different than the "normal" population. Color outliers include young sources, subdwarfs, binaries (both spectroscopic and visual), objects with uncertain spectral types, and objects with contaminated or suspect photometry. We discuss each of these in more detail below. All of the above samples are excluded from the list of objects used to determine typical UHS colors and absolute magnitudes of L, T, and Y dwarfs in Sections 3.5 and 3.6.

3.1. Binaries

Binaries often stand out compared to the normal field sequence on color-spectral type and color–magnitude diagrams (CMDs). L, T, and Y dwarf binaries in the UHS sample have generally been found in two ways, high angular-resolution imaging (e.g., Reid et al. 2001) and spectral decomposition (e.g., Burgasser et al. 2010). We searched for evidence of resolved or spectral binarity in the literature for the entire UHS sample. Twenty-four objects were found to be resolved binaries (Reid et al. 2001, 2006; Bouy et al. 2003; Gizis et al. 2003; Burgasser et al. 2005, 2006b, 2009; Liu et al. 2006, 2012; Siegler et al. 2007; Stumpf et al. 2010; Artigau et al. 2011;

Radigan et al. 2013). Note that we do not exclude wide binaries ($\gtrsim 1''$) from color or absolute magnitude relations because they are generally well-resolved in the photometric surveys used in this study. For spectroscopic binaries, we only include those objects with strong evidence of binarity, and find 24 spectral binaries in the UHS sample (Burgasser 2007; Burgasser et al. 2010; Geißler et al. 2011; Kirkpatrick et al. 2011; Mace et al. 2013; Bardalez Gagliuffi et al. 2014, 2019; Best et al. 2015; Robert et al. 2016; Kellogg et al. 2017; Zhang et al. 2021). All resolved and strong spectroscopic binary candidates are flagged in Table A1.

A newly available indicator of binarity is the renormalized unit weight error (RUWE) from Gaia, which is a measure of the astrometric goodness of fit (Lindegren et al. 2018). RUWE values >1.4 are generally indicative of an object being a close binary (Lindegren et al. 2018). Twenty-two objects in our sample have a Gaia RUWE value >1.4, which are flagged in Table A1. This list includes the known, resolved binaries 2MASS J07003664+3157266AB (L3+L6.5, sep $\approx 0''2$; Reid et al. 2006; Dupuy & Liu 2012), 2MASSW 0856479+223518 (L3+?, sep $\approx 0''1$; Bouy et al. 2003), and Gl 417BC (L4.5 +L6, sep $\approx 0''07$; Bouy et al. 2003; Dupuy & Liu 2012). The sample of high-RUWE objects also includes spectroscopic binaries SDSS J080531.84+481233.0 (L4.5+T5; Burgasser 2007), SDSS J093113.23+280227.1 (L1.5+T2.5; Bardalez Gagliuffi et al. 2014), and 2MASS J11061197+2754225 (T0 +T4.5; Burgasser et al. 2010). Note that SDSS J080531.84 +481233.0 is also an astrometric binary (Dupuy & Liu 2012; Burgasser et al. 2016a; Sahlmann et al. 2020). Two known subdwarfs were also found to have high RUWE values: WISEA J043535.82+211508.9 (sdL0; Kirkpatrick et al. 2014) and 2MASS J14343616+2202463 (d/sdL1; this work). It is possible that the exceptionally high proper motions of these objects compared to their parallaxes led to uncertain fits, or perhaps they are indeed subdwarf binaries. Further investigation of these sources may be warranted. One additional wide companion was also found to have a RUWE value >1.4 (NLTT 44368B (L1.5); Deacon et al. 2014). Previous work has shown that wide companions are often found to be binaries themselves (Faherty et al. 2010; Law et al. 2010). NLTT 44368B could be another example of this class of objects.

3.2. Red Photometric Outliers

Young brown dwarfs (age $\lesssim 200$ Myr) often have redder near-infrared colors than field-age counterparts of the same spectral type (e.g., Kirkpatrick et al. 2008) due to their lower surface gravities. However, not all redder-than-usual objects show clear signs of youth in their spectra (e.g., Looper et al. 2008; Marocco et al. 2014). Eighty-one objects in the sample are flagged as young, red, or both in Table A1.

3.3. Blue Photometric Outliers

Low-metallicity objects (subdwarfs) often have unusually blue near-infrared colors compared to typical low-mass stars and brown dwarfs due to the enhanced collision induced absorption (CIA) from H_2 (e.g., Linsky 1969). However, not all low-temperature objects with blue colors are subdwarfs (e.g., Cushing et al. 2010). Forty-four objects in this sample are flagged as being a subdwarf, blue, or both in Table A1.
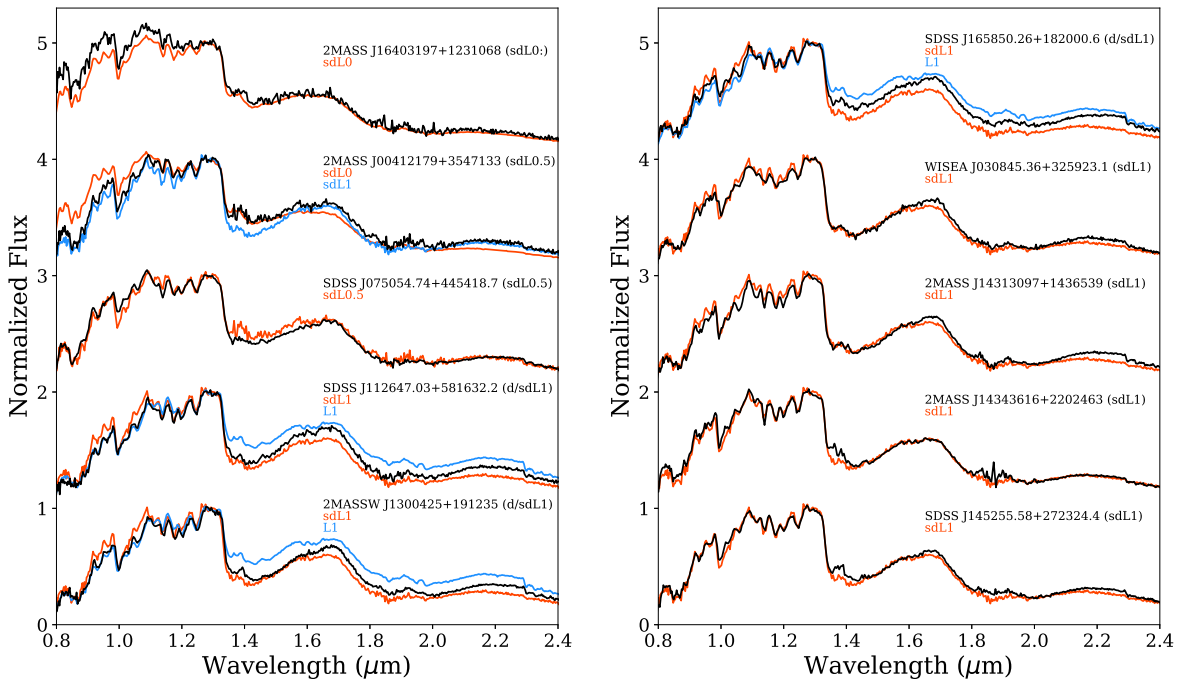
Figure 3. Objects with new (or updated) sdL classifications. Each spectrum is normalized to the *J*-band peak between 1.27 and 1.29 μm, and is offset by integer numbers for clarity. Spectral standards are plotted as orange or blue with types labeled in the figure.

3.4. Miscellaneous Outliers

The spectra of some low-temperature objects are denoted as "unusual" or "peculiar" compared to spectral standards and do not easily fit into a category of known unusual objects (e.g., young, old, binary). These objects are often labeled as "pec" or given a ":" to indicate an uncertain spectral type determination, though the latter can also be applied to low-signal-to-noise ratio (S/N) sources. All such objects are flagged in Table A1. Furthermore, a small subset of objects in this sample have poor or contaminated photometry from one of the additional photometric surveys (e.g., Pan-STARRS DR2, CatWISE 2020) and are thus unsuitable for inclusion in determining photometric relations. We also flag objects brighter than the nominal WFCAM saturation limit of ~11 mag (Hodgkin et al. 2009). Any objects with such photometry are flagged in Table A1 and are not included in any relations that use that particular photometry.

3.5. Colors

Determining the typical colors of L, T, and Y dwarfs is useful for characterizing these objects in general and as templates to estimate the properties of newly discovered objects. For this study, we determine the color versus spectral type trends for several commonly used colors involving UHS photometry: $J - K$, $y_{PS1} - J$, $J - W2$ and $K - W2$, as shown in Figure 4. For colors that do not use UHS photometry, see previous studies for Pan-STARRS, WISE, or Gaia specific color information (e.g., Kirkpatrick et al. 2011; Best et al. 2018; Smart et al. 2019). The median colors as a function of spectral type are provided in Table 4. Note that we do not include objects flagged as young, red, subdwarf, blue, binary (spectroscopic or close visual), having uncertain or peculiar types, or poor/contaminated photometry. The uncertainties listed in the table are the 16 and 84 percentile ranges, and are only given when $\geqslant 5$ objects are available for a particular spectral subtype. When <5 objects are available for a particular subtype, we list only the median value.

3.6. CMDs

Color–magnitude diagrams are also useful for characterizing low-temperature samples. They are also used as a tool for finding relationships that can be extended to objects without measured parallaxes to determine photometric distances. We have gathered measured parallaxes for every object in our sample, which are provided in Table A1 (Dahn et al. 2002, 2017; Tinney et al. 2003; Vrba et al. 2004; Schilbach et al. 2009; Dupuy & Liu 2012, 2017; Manjavacas et al. 2013; Smart et al. 2013; Zapatero Osorio et al. 2014; Dupuy et al. 2015; Liu et al. 2016; Sahlmann et al. 2016; Gaia Collaboration et al. 2018, 2023; Kirkpatrick et al. 2019, 2021; Lodieu et al. 2019; Best et al. 2020; Zhang et al. 2021). If more than one parallax measurement is available for a particular object, then we use whichever has the smallest uncertainty.

Absolute *J*- and *K*-band magnitudes versus spectral type trends are shown in Figure 5. As with the color-spectral type trends, we do not include objects flagged as young, red, subdwarf, blue, binary (spectroscopic or close visual), having uncertain or peculiar types, or poor/contaminated photometry in Table A1. In addition, we require parallax S/N > 10 and a photometric S/N > 5. We fit the trends for *J* and *K* with a weighted fifth order polynomial and give the coefficients of the fits in Table 5.

4. Astrometry

To measure the proper motions for known L, T, and Y dwarfs in the UHS survey, we required both a *J*- and *K*-band detection in the UHS DR2 catalog, which ensures a sufficient time baseline for a proper motion measurement. Out of the full 966-object sample, 14 sources have *K*-band detections but no corresponding *J*-band detection. While the *J*-band UHS survey
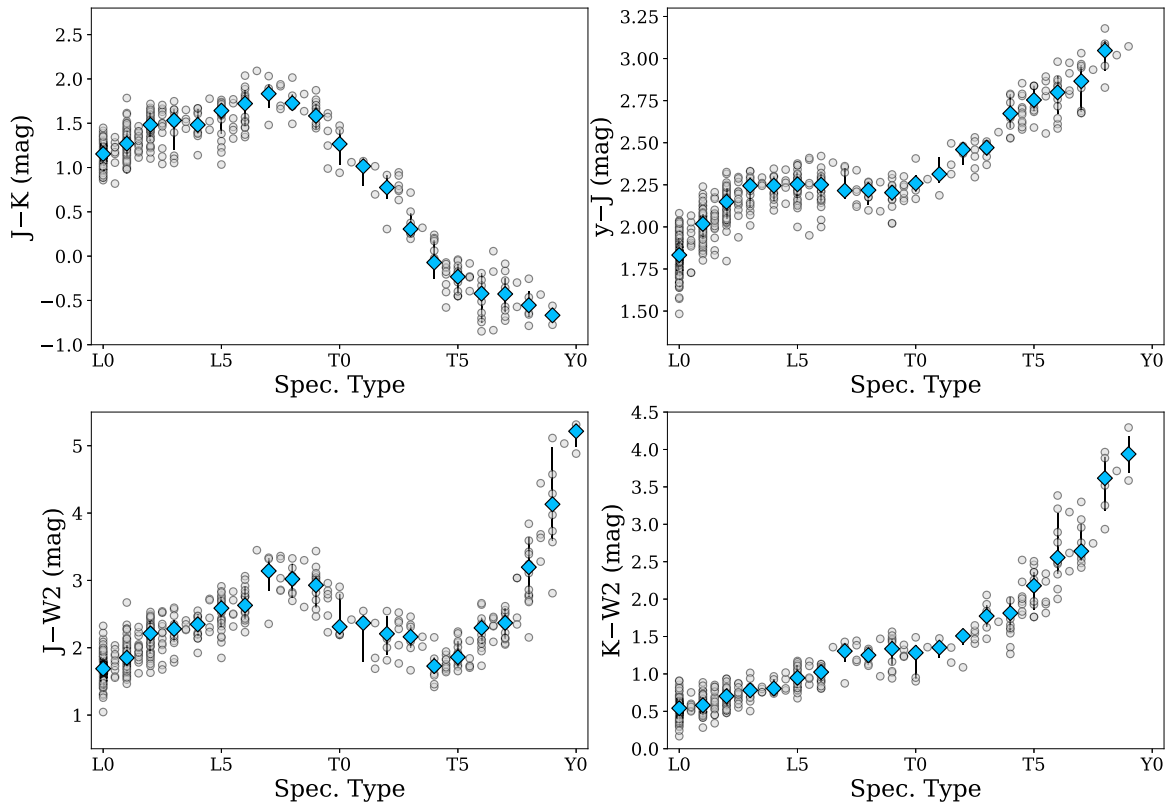
Figure 4. UHS colors ($J - K$, $y - J$, $J - $W2, and $K - $W2) as a function of spectral type. Median colors for integer types are shown as blue diamonds with errorbars showing the 16 and 84 percentile intervals and values presented in Table 4.

area is generally more complete, there are some small regions where there is K-band coverage and no J-band coverage. All 14 K-only sources are due to these small coverage differences. There are a total of 172 objects that have J-band detections but no corresponding K-band detection. Some of these are due to the more complete coverage of the J-band survey compared to K, which should be filled in with future UHS data releases. However, a significant fraction of the J-only sample has K-band coverage but remain undetected. These objects typically have spectral types $\gtrsim$T5, where $J - K$ colors turn especially blue.

The formal data releases of UHS are astrometrically calibrated against 2MASS. Bright sources in 2MASS have an astrometric accuracy of around 100 mas and lack proper motions (Skrutskie et al. 2006). To improve the astrometry, we have recalibrated each pawprint (a pawprint is the set of four images, one for each detector in the camera, for a single exposure) from the wide-field camera (WFCAM; Casali et al. 2007) against Gaia DR3, which has better than 1 mas astrometric accuracy, including proper motions and parallaxes, to $G \sim 20$ Gaia Collaboration et al. (2023). Furthermore, distortions in the WFCAM focal plane were removed by generating residual maps and applying those corrections. Separate residual maps were used for UHS-J and UHS-K, but each map was found to be stable throughout the survey. The rms residual between the recalibrated coordinates and Gaia for the bright stars used for the recalibrations is typically around 8 mas, with most better than 15 mas.

The recalibrated J- and K-band positions are then used to derive proper motions. For the objects with both J- and K-band detections (782 objects total), the median time baseline is ~5.1 yr between observations. If a matching Pan-STARRS detection is found, then its position is also used in deriving the proper motions. Each position is weighted by its inverse variance in the proper motion calculation. Gaia positions are not used because if a given object has a Gaia match, then the Gaia proper motion is preferred over the proper motions calculated here. All of the proper motions derived in this way are provided in Table A1.

To validate and evaluate the performance of the proper motions determined using UHS data, we compare our measurements to three different sources: Gaia DR3 (Gaia Collaboration et al. 2023), CatWISE 2020 (Marocco et al. 2021), and the Pan-STARRS derived proper motions in Best et al. (2018). The main results of this comparison are shown in Figure 6.

We find 291 objects from our proper motion sample that have proper motions in Gaia DR3 (Gaia Collaboration et al. 2023), as shown in the top panels of Figure 6. The vast majority of these sources have higher precision measurements in Gaia compared to our UHS proper motions (283/291; 97.2%). We find generally good agreement, with 80.8% of objects having both proper motion components within 3σ of Gaia DR3 measurements.

We find 774 objects from our proper motion sample with proper motions in CatWISE 2020 (Marocco et al. 2021), as shown in the middle row of Figure 6. Of these, the UHS derived proper motions have a higher precision for 755 objects (97.5%). Again, we generally find good agreement, with 88.4% of objects in common having both proper motion components within 3σ.

Table 4
Median Colors For L, T, and Y Dwarfs

Spectral Type	N	$J - K$ (mag)	N	$y - J$ (mag)	N	$J - W2$ (mag)	N	$K - W2$ (mag)
L0–L0.5	218	$1.15^{+0.10}_{-0.10}$	263	$1.83^{+0.10}_{-0.09}$	263	$1.69^{+0.15}_{-0.14}$	219	$0.54^{+0.09}_{-0.09}$
L1–L1.5	112	$1.27^{+0.14}_{-0.13}$	127	$2.02^{+0.06}_{-0.08}$	125	$1.85^{+0.18}_{-0.14}$	113	$0.58^{+0.10}_{-0.08}$
L2–L2.5	56	$1.48^{+0.14}_{-0.18}$	67	$2.15^{+0.08}_{-0.10}$	67	$2.21^{+0.18}_{-0.30}$	57	$0.70^{+0.11}_{-0.13}$
L3–L3.5	15	$1.53^{+0.12}_{-0.34}$	19	$2.24^{+0.05}_{-0.13}$	19	$2.28^{+0.13}_{-0.18}$	15	$0.78^{+0.04}_{-0.10}$
L4–L4.5	14	$1.48^{+0.18}_{-0.10}$	18	$2.25^{+0.05}_{-0.09}$	18	$2.35^{+0.15}_{-0.17}$	15	$0.81^{+0.12}_{-0.03}$
L5–L5.5	32	$1.64^{+0.07}_{-0.26}$	36	$2.25^{+0.10}_{-0.10}$	35	$2.59^{+0.16}_{-0.27}$	30	$0.95^{+0.17}_{-0.13}$
L6–L6.5	21	$1.72^{+0.15}_{-0.26}$	22	$2.25^{+0.06}_{-0.10}$	21	$2.63^{+0.27}_{-0.20}$	20	$1.02^{+0.07}_{-0.14}$
L7–L7.5	9	$1.83^{+0.10}_{-0.16}$	10	$2.22^{+0.13}_{-0.05}$	10	$3.14^{+0.19}_{-0.29}$	9	$1.30^{+0.11}_{-0.14}$
L8–L8.5	9	$1.73^{+0.10}_{-0.07}$	10	$2.22^{+0.05}_{-0.09}$	10	$3.02^{+0.23}_{-0.28}$	9	$1.25^{+0.08}_{-0.14}$
L9–L9.5	18	$1.58^{+0.13}_{-0.15}$	21	$2.20^{+0.05}_{-0.05}$	21	$2.93^{+0.14}_{-0.33}$	18	$1.34^{+0.13}_{-0.21}$
T0–T0.5	6	$1.27^{+0.16}_{-0.23}$	6	$2.26^{+0.05}_{-0.12}$	6	$2.31^{+0.49}_{-0.12}$	6	$1.28^{+0.10}_{-0.34}$
T1–T1.5	3	1.01	5	$2.31^{+0.10}_{-0.05}$	5	$2.37^{+0.09}_{-0.58}$	3	1.35
T2–T2.5	8	$0.77^{+0.14}_{-0.13}$	9	$2.46^{+0.04}_{-0.09}$	10	$2.21^{+0.26}_{-0.31}$	7	$1.51^{+0.07}_{-0.12}$
T3–T3.5	8	$0.31^{+0.18}_{-0.05}$	8	$2.47^{+0.03}_{-0.05}$	9	$2.16^{+0.17}_{-0.16}$	8	$1.77^{+0.15}_{-0.14}$
T4–T4.5	17	$-0.07^{+0.25}_{-0.18}$	18	$2.67^{+0.11}_{-0.08}$	18	$1.73^{+0.13}_{-0.12}$	16	$1.81^{+0.21}_{-0.25}$
T5–T5.5	16	$-0.23^{+0.14}_{-0.20}$	17	$2.75^{+0.08}_{-0.07}$	19	$1.86^{+0.24}_{-0.14}$	16	$2.18^{+0.18}_{-0.32}$
T6–T6.5	13	$-0.42^{+0.23}_{-0.33}$	16	$2.80^{+0.10}_{-0.13}$	19	$2.29^{+0.15}_{-0.24}$	14	$2.56^{+0.59}_{-0.22}$
T7–T7.5	12	$-0.43^{+0.18}_{-0.20}$	11	$2.87^{+0.10}_{-0.18}$	17	$2.37^{+0.21}_{-0.23}$	11	$2.64^{+0.36}_{-0.12}$
T8–T8.5	6	$-0.55^{+0.16}_{-0.13}$	6	$3.05^{+0.06}_{-0.12}$	19	$3.20^{+0.28}_{-0.44}$	6	$3.62^{+0.28}_{-0.43}$
T9–T9.5	2	-0.67	1	3.07	8	$4.13^{+0.85}_{-0.54}$	2	3.94
Y0	0	...	0	...	3	5.22	0	...

Note. This table gives the number of objects followed by median colors or L, T, and Y dwarfs in UHS. Uncertainties are the 16 and 84 percentile ranges, and are only calculated when $N \geqslant 5$.

Because the proper motions of Pan-STARRS DR2 are not publicly available, we compare to the Pan-STARRS derived motions determined in Best et al. (2018), which can be seen in the bottom row of Figure 6. There are 293 objects with proper motions in Best et al. (2018) in common with our UHS proper motion sample. We find higher precision from the UHS derived proper motions for 262 (89.4%) of these objects. There is a good agreement, with 87.4% of objects in common having both proper motion components within 3σ.

We further searched the literature and available catalogs to find the most precise proper motions that exist for all of the objects in the full UHS LTY sample. Any proper motion found that is more precise than available proper motions from this work, Gaia DR3, CatWISE 2020, and Best et al. (2018) is provided in Table A1. We find that our UHS derived proper motions are the most precise measurements for 381 of the 966 objects in this work (∼39%). For the investigations in Section 5, we use the best available proper motions.

5. Objects of Interest

5.1. Young Moving Group Members

Nearby associations and moving groups in the solar neighborhood serve as important laboratories for testing stellar and substellar evolutionary theory. Any L, T, or Y dwarf that can be tied to such a group with a well-determined age becomes an important benchmark because ages are typically difficult to determine for field L, T, and Y dwarfs. Nearby groups tend to have distinct kinematics, and several tools have been developed to determine the probabilities of belonging to various nearby groups based on kinematics alone.

The best available astrometry for all objects in this sample was input into BANYAN Σ (Gagné et al. 2018) and LACEwING (Riedel et al. 2017) to determine potential moving group or association membership. BANYAN Σ evaluates potential membership for 29 groups in the solar neighborhood via a Bayesian classifier and a candidate's available astrometric information (i.e., position, proper motion, parallax, and radial velocity). Alternatively, LACEwING uses a frequentist framework to compare the kinematic information of a candidate to 16 nearby moving groups. All of the groups included in LACEwING are also included in BANYAN Σ, although the lists of known members varies. For both BANYAN Σ and LACEwING, we choose a relatively conservative probability threshold value of ⩾80% for an object to be considered a candidate moving group or association member. For each object, we used UHS positions, the best available proper motion values (based on smallest uncertainties), and the highest-precision parallax (when available). If a parallax is not available, we use J-band photometric distances and corresponding uncertainties determined from Table 5. K-band photometric distances are used if measured parallaxes and J-band photometry are unavailable.

Eighty-seven objects were found to have membership probabilities of 80% or larger from BANYAN Σ, LACEwING, or both. Meanwhile, 54 of these are either known members or previously suggested candidate members. We discuss each group for which a member or candidate member was found, and evaluate potential membership for new candidates in the following sections.

5.1.1. The AB Doradus Moving Group

The AB Doradus Moving Group (ABDMG) was first identified in Zuckerman et al. (2004) and has an estimated age of 149^{+51}_{-19} Myr (Bell et al. 2015). Our search recovered nine
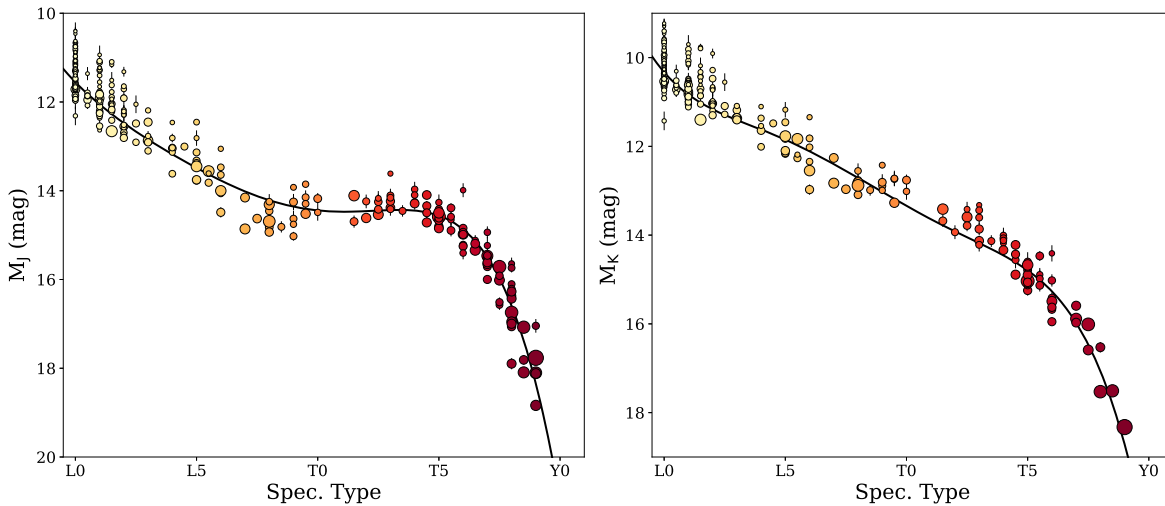
Figure 5. Absolute UHS *J*- and *K*-band magnitudes as a function of spectral type for L, T, and Y dwarfs observed as part of the UKIRT Hemisphere Survey. The symbol sizes represent distances, with larger symbols corresponding to closer distances. Colors correspond to spectral type. This figure does not include known close binaries (spectroscopic or resolved), young objects, subdwarfs, objects with uncertain types, objects designated "red," "blue," or "pec," or objects with a parallax S/N < 10.

known or previously suggested candidate ABDMG members and six new candidate members, which are listed in Table 6. The two recovered candidates are the wide companions LP 261-75B and HD 89744B. Liu et al. (2016) found the L 261-75AB system to most likely belong to the young field population and we adopt that result here, listing L 261-75B in the rejected members in Table 6. Furthermore, the primary to HD 89744B (HD 89744A) was once considered to be an AB Dor member but was later found to have an age of several Gyr, which is inconsistent with AB Dor membership (Schaefer et al. 2018). We adopt this result here and list HD 89744B in the list of rejected members. Recovered members include the very well-known low-mass members 2MASS J03552337+1133437 and 2MASSW J2244316+204343, as well as the planetary mass companion GU Psc b (Naud et al. 2014). Our UHS proper motion of GU Psc b is the most precise measured so far for this object. Using COMOVER (Gagné et al. 2021) and Gaia DR3 astrometry for the primary, we find a co-moving probability of 98.6% of GU Psc and GU Psc b without using a distance estimate for the b component. If we include the *K*-band distance estimate of 44 ± 8 pc (determined using the relations given in Table 5), then we find a co-moving probability of 99.98%. While the physical association of GU Psc and GU Psc b is not in doubt, our measured proper motion for the b component is consistent with and reaffirms the physical association of this pair.

Of the six new candidate members identified in this work, we reject three of them as possible ABDMG members. CWISE J043309.36+100902.3 returns a significant probability of ABDMG membership from both BANYAN and LACEwING; however, the best proper motion values for this object, which come from Meisner et al. (2020b), have relatively large uncertainties ($\sim$35 mas yr^{-1}). A more precise proper motion is needed for this object to consider it to be an ABDMG candidate member. PSO J004.1834+23.0741 was returned as a high-probability ABDMG member from LACEwING but has a 0% probability of ABDMG membership from BANYAN Σ, and we therefore do not consider this object as a new candidate ABDMG member. WISE J111838.70+312537.9 is a widely separated companion to the quadruple star system ξ Ursae

Majoris, which was found to have an age of several Gyr (Wright et al. 2013), and is thus not an ABDMG member

Both 2MASSI J0409095+210439 and 2MASS J06143818 +3950357 are returned as high-probability ABDMG members according to BANYAN Σ, with non-zero probabilities of ABDMG from LACEwING as well. Both objects have well-measured parallaxes, which bolsters their potential membership. We retrieved the IRTF/SpeX spectrum of 2MASSI J0409095+210439, and while it has no clear spectral features indicating a low surface gravity, we note that it is slightly red compared to the L3 and L4 standards, which is a common feature of known young brown dwarfs. The near-infrared spectrum of 2MASS J06143818+3950357 presented in Mužić et al. (2012) is a good match to the L9 standard with no obvious signs of low-gravity. LACEwING also gives a high probability of belonging to the Hyades for this object (88.0%), but we find membership unlikely in Section 5.1.6. Higher-resolution spectroscopy of these objects would allow for a deeper investigation of gravity sensitive features and radial velocity measurements, which would firmly assess the membership status for these L dwarfs. Both objects are flagged as potentially young in Table A1.

PSO J057.2893+15.2433 is a red L7 discovered in Best et al. (2015), who found a strong probability of membership in the β Pictoris Moving Group (BPMG). Using our measured UHS proper motion and a *J*-band photometric distance, we instead find a high probability of ABDMG membership. We note, however, that *J*-band photometric distances tend to underestimate actual distances for red L dwarfs because of their unusual SEDs (Schneider et al. 2023). Using the *K*-band photometric distance for this object (31 ± 5 pc, compared to 48 ± 8 pc for *J*), we find ambiguous membership from BANYAN Σ–54.1% membership probability in ABDMG and 37.9% membership probability in BPMG. We retain this object as an ABDMG candidate member in need of parallax and radial velocity measurements.

5.1.2. The Argus Association

The Argus Association (ARG) was originally identified in Torres et al. (2008), though this original group was heavily

Table 5
Coefficients of Absolute Magnitude Polynomial Fits

x	y	c_0	c_1	c_2	c_3	c_4	c_5	Rms
SpT	M_J	−2.35283E+01	1.01992E+01	−1.21981E+00	7.54721E-02	−2.31859E-03	2.78465E-05	0.406
SpT	M_K	−5.36375E+01	1.87805E+01	−2.17131E+00	1.24194E-01	−3.47013E-03	3.79874E-05	0.399

Note. These polynomials take the form.

$$y = \sum_{i=0}^{n} c_i x^i,$$

where spectral type L0 = 10, T0 = 20, and Y0 = 30.

contaminated, leading Zuckerman (2019) to reexamine and redefine the membership of this group and give an age of 40–50 Myr. Our search recovered two known L-type members, and returned seven new candidate members, as summarized in Table 7.

The new ARG candidate 2MASS J04070752+1546457 is a strong Hα emitter (Reid et al. 2008) and a rapid rotator (Tannock et al. 2021). Despite being a high-probability ARG member from BANYAN Σ and a moderate-probability member according to LACEwING, the predicted radial velocities ($\sim$21.6 km s^{-1} and $\sim$21.1 km s^{-1}, respectively) do not agree with the measured radial velocity from Tannock et al. (2021; 43.4 ± 2.1 km s^{-1}). We therefore reject 2MASS J04070752+1546457 as an ARG member.

The new candidate CWISE J062317.13+263129.7 was discovered by Scholz (2020) using Gaia data and given a photometric type of L4.5 ± 2.5. This object was spectroscopically classified in Kirkpatrick et al. (2021), and labeled "L3 pec (composite?)." As seen in Figure 10 of that paper, the spectrum is a decent match to the L3 standard at J but much redder at H and K, possibly indicating a low surface gravity. This object was not evaluated as a potential moving group member in Kirkpatrick et al. (2021) because that investigation was limited to objects determined to be within 20 pc. A radial velocity is needed to establish ARG membership for this object.

BANYAN Σ returned high membership ARG probabilities for 2MASS J15311344+1641282, 2MASS J17153111 +1054108, SDSS J202820.32+005226.5, and 2MASS J23313131+2041273. The IRTF/SpeX spectra of these sources show no obvious signs of low surface gravity, but there is no clear reason to rule these objects out as candidates. More information is needed to establish ARG or field membership for these objects. We retain all four objects as ARG candidates.

SDSS J135923.99+472843.2 was discovered in Knapp et al. (2004) and assigned a near-infrared type of L8.5. There is no previous evidence of youth for this object in the literature, but it has not been studied in great detail. Our UHS proper motion suggests ARG membership and we keep it as a candidate.

We consider CWISE J062317.13+263129.7, SDSS J135923.99 +472843.2, 2MASS J15311344+1641282, 2MASS J17153111 +1054108, SDSS J202820.32+005226.5, and 2MASS J23313131+2041273 to be potential new ARG members, which are flagged as possibly young in Table A1.

Finally, we mention 2MASS J10271549+5445175, which was determined to have a spectral type of L2 VL-G in Section 2. BANYAN Σ returns a 46.5% probability for ARG membership, with no other groups having probabilities >1%. The predicted distance for ARG if a member is $\sim$53.4 pc,

which is in good agreement with the photometric J-band distance for this object of 50 ± 9 pc (note that no UHS K-band photometry is available for this source). Because the spectrum shows signs of low gravity and the estimated distance for this object aligns well with ARG membership, we consider this object to be an ARG candidate member in need of a more detailed investigation.

5.1.3. The β Pictoris Moving Group

The Beta Pictoris Moving Group (BPMG) was identified in Zuckerman et al. (2001), with the most recent age determination of 20.4 ± 2.5 Myr (Couture et al. 2023). Our search returned one previously known candidate BPMG member (CWISE J050626.96+073842.4; Schneider et al. 2023). No new BPMG candidates were found in our search.

5.1.4. The Carina-Near Moving Group

The Carina-Near Moving Group (CARN) was identified in Zuckerman et al. (2006), and has an age estimate of 200 ± 50 Myr (Zuckerman et al. 2006). Our search returned six known L- and T-type members or candidate members, as summarized in Table 8. No new CARN candidates were found in this search.

5.1.5. The Coma Ber Cluster

The Coma Ber Cluster (CBER) is the second closest open cluster to the Sun after the Hyades, and has recent age estimates of 700–800 Myr (Tang et al. 2018; Martín et al. 2020; Sapozhnikov & Kovaleva 2021; Singh et al. 2021). Two CBER candidates were found in this search. Using the Gaia DR3 proper motion and parallax of SDSS J125108.28+155911.1 (L0; Kiman et al. 2019), we find a high probability of CBER membership from LACEwING (88.0%), though BANYAN Σ returns a 0% probability of CBER membership. If SDSS J125108.28+155911.1 is a CBER member, then it would exist outside of the tidal radius. By comparing the Cartesian XYZ coordinates of SDSS J125108.28+155911.1 found from Gaia DR3 astrometry (7.5, −11.8, 70.9 pc) to the coordinates of core and tidal tail members from Tang et al. (2019), we find that SDSS J125108.28+155911.1 would have the lowest Z value of all candidate members by $\sim$6.4 pc. We therefore suggest that CBER membership is unlikely for SDSS J125108.28 +155911.1.

The other CBER candidate is 2MASS J13264464+3627407 (L2; Kellogg et al. 2017). Using the UHS proper motion and J-band photometric distance of this source (no parallax is available), LACEwING returns a 93.0% probability of CBER membership, while BANYAN Σ does not find a significant probability of CBER membership. We retain 2MASS
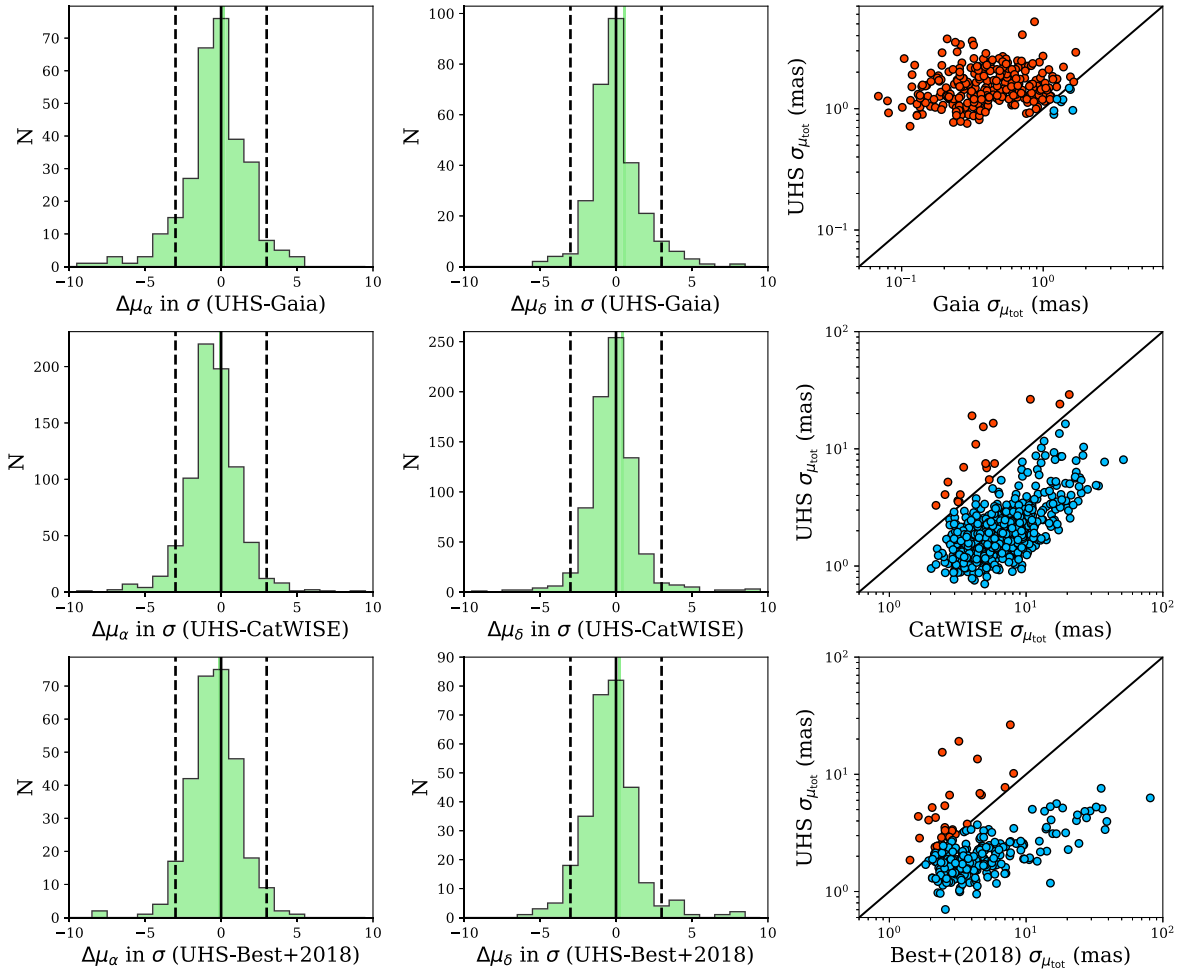
Figure 6. A comparison of proper motions derived from UHS positions in this work to Gaia DR3 (top row), CatWISE 2020 (middle row), and Pan-STARRS derived proper motions in Best et al. (2018; bottom row). The left-hand panels show histograms of the difference between μ_α measurements in combined σ, with dashed-black lines indicating 3σ differences between measurements. The middle panels show similar histograms for μ_δ. The right-hand panels compare the uncertainty values of the total proper motions for objects, with red symbols indicating smaller uncertainties in either Gaia DR3, CatWISE 2020, or Best et al. (2018) compared to UHS proper motions, and blue symbols indicating smaller uncertainties for UHS proper motions. These are separated by a solid diagonal line indicating 1-to-1 values.

J13264464+3627407 as a tentative candidate requiring additional validation. We do not flag this object as young in Table A1 because brown dwarfs with ages of ∼700 Myr are not known to be readily distinguishable from the field L and T population.

5.1.6. The Hyades Cluster

The Hyades is the closest known open cluster to the Sun, and has an age of ∼650 Myr (e.g., Lodieu et al. 2019). Twenty-seven previously suggested L- and T-type Hyades members were recovered in our search, in addition to 18 new candidate members, as summarized in Table 9. Of the recovered members, we highlight 2MASS J01311838+3801554, 2MASS J01472702+4731142, and 2MASSW J0208183+254253. 2MASS J01311838+3801554 and 2MASS J01472702 +4731142 were returned as strong Hyades candidates from LACEwING, with weak probabilities from BANYAN Σ, while 2MASSW J0208183+254253 had a strong LACEwING probability and moderately high probability from BANYAN Σ. All three of these objects are included in the list of possible Hyades cluster members from Gaia Collaboration et al. (2021). These objects exist well outside of the core radius of the Hyades cluster, with distances of 30–38 pc from the cluster

center (Gaia Collaboration et al. 2021), which is why these objects were missed as Hyades members in previous searches and the recent compilation of L- and T-type Hyades members in Schneider et al. (2022).

Fourteen objects (i.e., WISEA J015812.03+323157.9, SDSS J020608.97+223559.2, 2MASSW J0208236+273740, WISEA J022721.93+235654.3, 2MASSW J0242435+160739, UGCS J030013.86+490142.5, WISEPA J030533.54+395434.4, 2MASSW J0310599+164816, PSO J049.1124+17.0885, 2MASS J03302948+3910242, SIMP J03570493+1529270, WISEA J041743.13+241506.3, PSO J070.3773+04.7333, and 2MASS J06143818+3950357) were returned as high-probability Hyades members from LACEwING, but have a 0% probability of belonging to the Hyades from BANYAN Σ. The directions of their proper motion components do not align with known Hyades members, which is confirmed via a convergent point analysis. We find that all of these objects are unlikely to be Hyades members.

SDSS J011912.22+240331.6 (T2.5; Burgasser et al. 2010) is a new candidate Hyades member that has been identified in this work. Although it is suggested as a binary candidate based on spectral decomposition (Burgasser et al. 2010; Bardalez Gagliuffi et al. 2014; Ashraf et al. 2022), it remains unresolved (Radigan et al. 2013; Bardalez Gagliuffi et al. 2014). Using the convergent point of the Hyades from Madsen et al. (2002) and

Table 6
AB Dor Members and Candidate Members

Name	Sp. Type	References	μ_α (mas yr^{-1})	μ_δ (mas yr^{-1})	References	ϖ[a] (mas)	References	BANYAN (%)	LACEwING (%)	References[b]
Recovered Members										
GU Psc b	T3.5	1	77.3 ± 13.2	−101.0 ± 13.1	2	21.01 ± 0.03[c]	3	92.0	13.0	1,4,5
2MASS J03552337+1133437	L3–L6γ	6	223.18 ± 0.59	−631.30 ± 0.37	3	109.14 ± 0.48	3	99.7	87.0	7,8,9,10,11,12
2MASS J04203904+2355502	L1	13	44.72 ± 0.69	−168.61 ± 0.46	3	25.17 ± 0.60	3	98.3	50.0	14,15
WISE J064205.58+410155.5	L9 (red)	16	−2.0 ± 1.2	−383.1 ± 1.2	17	62.6 ± 3.1	17	85.9	66.0	17
PSO J318.4243+35.1277	L1	4	111.73 ± 0.25	−76.86 ± 0.27	3	32.71 ± 0.30	3	98.7	30.0	4,18
2MASSW J2244316+204343	L6-L8γ	6	230.3 ± 0.9	−234.8 ± 1.0	12	58.7 ± 1.0	12	99.7	54.0	4,10,11,12,19
PSO J358.5527+22.1393	L2	4	101.22 ± 0.67	−89.30 ± 0.40	3	22.98 ± 0.61	3	93.4	21.0	4,18
New Candidate Members										
PSO J057.2893+15.2433	L7 (red)	16	72.33 ± 3.83	−133.91 ± 3.58	2	[21 ± 4]	2	89.8	59.0	16
2MASSI J0409095+210439	L3.5	20	92.51 ± 1.07	−171.28 ± 0.81	3	31.49 ± 0.92	3	89.9	74.0	...
2MASS J06143818+3950357	L9	21	−31.9 ± 1.7	−264.9 ± 1.8	22	44.0 ± 2.6	22	85.8	58.0	...
Rejected Candidate Members										
PSO J004.1834+23.0741	T0	16	405.4 ± 2.1	61.8 ± 2.5	22	38.4 ± 3.3	22	0.0	86.0	...
CWISE J043309.36+100902.3	T8	17	174 ± 34	−384 ± 36	23	[53 ± 9]	2	88.7	68.0	...
LP 261-75B	L6:	12	−94.0 ± 2.4	−164.3 ± 2.7	12	29.6 ± 2.8	12	83.7	25.0	12
HD 89744B	L0.5	24	−119.22 ± 0.65	−140.39 ± 0.46	3	26.01 ± 47	3	91.6	13.0	25
WISE J111838.70+312537.9	T8.5	26	−405.1 ± 8.1	−588.6 ± 9.4	27	114.49 ± 0.43[d]	3	84.0	39.0	...

Notes.

[a] Parallaxes in square brackets are photometric.

[b] References in the final column are the relevant works that have previously evaluated, suggested, or determined moving group membership.

[c] The parallax for this object comes from the primary star GU Psc.

[d] The parallax for this object comes from the primary star ξ Uma.

References. (1) Naud et al. (2014); (2) This work; (3) Gaia Collaboration et al. (2023); (4) Aller et al. (2016); (5) Zhang et al. (2021); (6) Gagné et al. (2015a); (7) Faherty et al. (2013); (8) Liu et al. (2013); (9) Zapatero Osorio et al. (2014); (10) Gagné et al. (2014); (11) Faherty et al. (2016); (12) Liu et al. (2016); (13) Luhman (2006); (14) Kraus et al. (2017); (15) Gagné et al. (2018); (16) Best et al. (2015); (17) Kirkpatrick et al. (2021); (18) Gagné & Faherty (2018); (19) Vos et al. (2018); (20) Bardalez Gagliuffi et al. (2014); (21) Mužić et al. (2012); (22) Best et al. (2020); (23) Meisner et al. (2020b); (24) Schneider et al. (2014); (25) Schaefer et al. (2018); (26) Wright et al. (2013); (27) Marocco et al. (2021).

Table 7
Argus Members and Candidate Members

Name	Sp. Type	References	μ_α (mas yr^{-1})	μ_δ (mas yr^{-1})	References	ϖ[a] (mas)	References	BANYAN (%)	LACEwING (%)	References[b]
Recovered Members										
2MASSW J0045214+163445	L2 VL-G	1	359.07 ± 0.20	-47.91 ± 0.14	2	65.406 ± 0.175	2	99.1	67.0	3,4,5,6,7,8,9,10
SDSS J213240.36+102949.4	L4: β	11	107.94 ± 2.23	27.67 ± 2.30	12	$[23 \pm 4]$	12	84.2	5.0	6,11,13
New Candidate Members										
CWISE J062317.13+263129.7	L3 pec	10	-8.56 ± 0.54	-130.33 ± 0.39	2	48.61 ± 0.48	2	99.1	52.0	...
SDSS J135923.99+472843.2	L8.5	14	-158.27 ± 2.36	59.05 ± 2.51	12	$[28 \pm 5]$	12	85.1	0.0	...
2MASS J15311344+1641282	L2	12	-89.74 ± 1.43	29.70 ± 0.99	2	26.75 ± 1.12	2	96.2	0.0	...
2MASS J17153111+1054108	L6	15	-38.59 ± 2.93	2.68 ± 2.76	12	$[25 \pm 4]$	12	88.7	6.0	...
SDSS J202820.32+005226.5	L2	16	96.04 ± 0.54	-11.16 ± 0.44	2	35.14 ± 0.45	17	98.3	44.0	...
2MASS J23313131+2041273	L3.5	2	124.74 ± 2.16	-10.79 ± 2.22	12	$[26 \pm 5]$	12	89.6	0.0	...
Rejected Candidate Members										
2MASS J04070752+1546457	L4 (red)	12	74.9 ± 1.5	-64.3 ± 1.1	7	28.9 ± 1.3	10	84.6	32.0	...

Notes.
[a] Parallaxes in square brackets are photometric.
[b] References in the final column are the relevant works that have previously evaluated, suggested, or determined moving group membership.

References. (1) Allers & Liu (2013); (2) Gaia Collaboration et al. (2023); (3) Gagné et al. (2014); (4) Zapatero Osorio et al. (2014); (5) Gagné et al. (2015b); (6) Faherty et al. (2016); (7) Liu et al. (2016); (8) Riedel et al. (2019); (9) Ujjwal et al. (2020); (10) Kirkpatrick et al. (2021); (11) Gagné et al. (2015a); (12) This work; (13) Vos et al. (2019); (14) Knapp et al. (2004); (15) Kellogg et al. (2017); (16) Burgasser et al. (2010); (17) Dahn et al. (2017).

Table 8
Carina-Near Members and Candidate Members

Name	Sp. Type	References	μ_α (mas yr^{-1})	μ_δ (mas yr^{-1})	References	ϖ (mas)	References	BANYAN (%)	LACEwING (%)	References[a]
Recovered Members										
PSO J004.6359+56.8370	T4.5	1	375.9 ± 3.2	10.4 ± 2.7	1	46.5 ± 3.9	1	89.7	0.0	2
WISE J003110.04+574936.3	L9	3	521.8 ± 1.5	-18.3 ± 1.6	4	71.0 ± 3.2	4	97.6	0.0	5
WISE J031624.35+430709.1	T8	6	375.5 ± 0.9	-227.4 ± 0.9	4	74.7 ± 2.1	4	94.4	0.0	2
2MASSI J1553022+153236	T6.5+T7.5	7	-385.8 ± 0.7	166.2 ± 0.9	7	75.1 ± 0.9	7	98.1	0.0	2,8
SDSSp J162414.37+002915.6	T6	9	-372.89 ± 1.60	-9.11 ± 1.95	10	90.9 ± 1.2	10	27.0	0.0	2,8
WISE J223617.59+510551.9	T5	3	719.1 ± 1.6	350.0 ± 1.8	11	102.8 ± 1.9	1	96.7	0.0	2,4,8

Note.

[a] References in the final column are the relevant works that have previously evaluated, suggested, or determined moving group membership.

References. (1) Best et al. (2020); (2) Zhang et al. (2021); (3) Best et al. (2013); (4) Kirkpatrick et al. (2021); (5) Vos et al. (2022); (6) Mace et al. (2013); (7) Dupuy & Liu (2012); (8) Hsu et al. (2021); (9) Burgasser et al. (2002); (10) Tinney et al. (2003); (11) This work.

Table 9
Hyades Members and Candidate Members

Name	Sp. Type	References	μ_α (mas yr^{-1})	μ_δ (mas yr^{-1})	References	ϖ[a] (mas)	References	BANYAN (%)	LACEwING (%)	References[b]
Recovered Members										
2MASS J01311838+3801554	L1.5	1	380.05 ± 0.45	−33.95 ± 0.43	2	40.92 ± 0.50	2	2.3	87.0	3
2MASS J01472702+4731142	L1	4	184.75 ± 1.26	−30.13 ± 1.16	2	20.85 ± 1.36	2	0.0	82.0	3
2MASSW J0208183+254253	L1.5	4	374.51 ± 0.34	−30.51 ± 0.34	2	43.10 ± 0.32	2	68.7	95.0	3
CWISE J031042.59+204629.3	L5	5	161.2 ± 2.0	−27.2 ± 2.1	6	[32 ± 6]	7	47.8	91.0	6
PSO J049.1159+26.8409	T2.5	8	201.1 ± 2.4	−52.8 ± 1.9	9	33.5 ± 3.1	9	85.6	96.0	6,10
PSO J052.2746+13.3754	T3.5	9	273.2 ± 2.0	−20.7 ± 2	9	44.3 ± 3.0	9	92.5	96.0	6,10
CWISE J033817.87+171744.1	L7	6	152.0 ± 3.5	−25.3 ± 3.3	6	[22 ± 4]	7	85.4	100.0	6
2MASS J03530419+0418193	L6 (red)	5	171.2 ± 3.1	35.8 ± 2.9	6	[31 ± 5]	7	5.7	100.0	6
SDSS J035308.54+103056.0	L1	11	128.75 ± 1.36	−19.61 ± 0.78	2	21.56 ± 0.95	2	0.0	100.0	12
Hya03	L1 pec (red)	13	110.25 ± 1.43	−13.06 ± 1.34	2	17.90 ± 1.20	2	72.6	100.0	6,12,14,15,16,17
WISEA J041232.77+104408.3	L5: (red)	18	129.5 ± 3.8	−5.5 ± 3.5	6	[16 ± 3]	7	72.9	97.0	6,18
Hya10	L1	16	123.6 ± 2.7	−17.8 ± 2.3	6	28.5 ± 3.9	17	99.2	100.0	6,14,17,17
2MASS J04183483+2131275	L5	19	141.5 ± 2.7	−45.7 ± 2.3	17	25.8 ± 2.9	17	98.3	100.0	6,12,17,19
CWISE J041953.55+203628.0	T4	6	109.4 ± 9.0	−35.8 ± 8.9	6	[27 ± 5]	7	97.9	100.0	6
2MASS J04241856+0637448	L4	12	138.8 ± 2.8	7.5 ± 2.9	6	[16 ± 3]	7	20.9	87.0	6,12
CWISE J042731.38+074344.9	L7	6	114.3 ± 3.5	5.5 ± 3.1	6	[23 ± 4]	7	96.2	100.0	6
CFHT-Hy-21	T1	20	82.1 ± 9.8	−15.5 ± 8.6	17	33.5 ± 12.7	17	74.7	83.0	16,17,20
CWISE J043018.70+105857.1	T4	6	106.3 ± 6.9	−10.7 ± 6.9	6	[25 ± 4]	7	98.7	100.0	6
CFHT-Hy-20	T2.5	21	142.6 ± 1.6	−16.5 ± 1.7	21	30.8 ± 1.5	21	98.7	100.0	6,10,17,20,21
Hya12	L6 (red)	7	100.2 ± 1.9	−15.1 ± 2.0	17	24.1 ± 2.1	17	99.5	100.0	6,14,16,17
WISEA J043642.75+190134.8	L6	18	113.5 ± 2.0	−42.1 ± 2.0	6	[25 ± 4]	7	99.1	100.0	6,18
PSO J069.7303+04.3834	T2	9	118.7 ± 3.5	11.7 ± 3.4	6	36.6 ± 5.7	9	86.1	94.0	6,10
CWISE J043941.41+202514.8	T3	6	80.8 ± 8.0	−30.3 ± 7.9	6	[25 ± 4]	7	88.5	99.0	6
WISEA J044105.56+213001.5	L5 (red)	18	97.7 ± 4.3	−43.6 ± 4.0	6	[16 ± 3]	7	84.6	99.0	6,18
Hya09	L2	16	76.3 ± 2.9	−17.7 ± 1.5	17	20.6 ± 2.5	17	96.9	100.0	6,14,16,17
Hya08	L0.5	16	88.63 ± 1.12	−17.45 ± 0.77	2	22.73 ± 0.88	2	99.0	100.0	6,14,16,17
CWISE J053204.60+111955.1	L7	6	72.5 ± 1.9	−30.2 ± 1.9	6	[41 ± 7]	7	59.7	94.0	6
New Candidate Members										
SDSS J011912.22+240331.6	T2.5	1	264.6 ± 1.5	5.5 ± 1.6	9	28.9 ± 2.9	9	1.4	91.0	...
WISEPA J020625.26+264023.6	L9 (red)	22	442.7 ± 2.1	−41.9 ± 2.3	20	52.1 ± 1.4	20	33.1	89.0	...
2MASSW J0228110+253738	L1	7	244.62 ± 0.21	−29.60 ± 0.42	23	30.03 ± 0.46	23	68.8	98.0	...
2MASSW J0306268+154514	L6.5	7	205.4 ± 3.5	−12.8 ± 3.7	7	[22 ± 4]	7	52.5	100.0	...
Rejected Candidate Members										
WISEA J015812.03+323157.9	L4.5	24	353.98 ± 2.31	−315.51 ± 2.05	7	[31 ± 5]	7	0.0	87.0	...
SDSS J020608.97+223559.2	L5.5	25	396.91 ± 2.63	−64.69 ± 2.36	7	[28 ± 5]	7	0.0	86.0	...
2MASSW J0208236+273740	L6	4	206.3 ± 2.4	−116.1 ± 2.8	7	21.3 ± 2.7	9	0.0	93.0	...
WISEA J022721.93+235654.3	L9	26	315.13 ± 3.34	−127.98 ± 3.22	7	[35 ± 6]	7	0.0	98.0	...
2MASSW J0242435+160739	L2 (sl. blue)	7	155.26 ± 1.76	−207.41 ± 1.65	2	21.31 ± 1.85	2	0.0	95.0	...
UGCS J030013.86+490142.5	T6.5	27	94.9 ± 48.8	−130.3 ± 52.0	28	[27 ± 5]	7	0.0	81.0	...
WISEPA J030533.54+395434.4	T6	22	273 ± 1.5	4.7 ± 1.5	9	27.8 ± 2.0	9	0.0	97.0	...
2MASSW J0310599+164816	L9 (sl. red)	7	242.5 ± 2.5	4.1 ± 1.9	2	36.9 ± 3.4	29	0.0	98.0	...
PSO J049.1124+17.0885	L9.5	8	267.8 ± 3.8	−104.9 ± 3.4	7	[31 ± 5]	7	0.0	89.0	...
2MASS J03302948+3910242	L7 pec (red)	5	67.23 ± 3.50	−116.79 ± 3.64	7	[21 ± 4]	7	0.0	87.0	...

14

Table 9
(Continued)

Name	Sp. Type	References	μ_α (mas yr^{-1})	μ_δ (mas yr^{-1})	References	ϖ^{a} (mas)	References	BANYAN (%)	LACEwING (%)	References[b]
SIMP J03570493+1529270	L1:: pec (blue)	13	96.94 ± 0.61	-286.36 ± 0.43	2	24.98 ± 0.59	2	0.0	98.0	...
WISEA J041743.13+241506.3	T6	26	394.76 ± 4.61	-508.76 ± 3.56	7	$[75 \pm 13]$	7	0.0	83.0	...
PSO J070.3773+04.7333	T4.5	8	212.5 ± 3.1	-105.7 ± 2.9	9	23.5 ± 4.9	9	0.0	95.0	...
2MASS J06143818+3950357	L9	30	-31.9 ± 1.7	-264.9 ± 1.8	9	44.0 ± 2.6	9	0.0	88.0	...

Notes.
[a] Parallaxes in square brackets are photometric.
[b] References in the final column are the relevant works that have previously evaluated, suggested, or determined moving group membership.

References. (1) Burgasser et al. (2010); (2) Gaia Collaboration et al. (2023); (3) Gaia Collaboration et al. (2021); (4) Schneider et al. (2014); (5) Kellogg et al. (2017); (6) Schneider et al. (2022); (7) This work; (8) Best et al. (2015); (9) Best et al. (2020); (10) Zhang et al. (2021); (11) Bardalez Gagliuffi et al. (2014); (12) Pérez-Garrido et al. (2018); (13) Robert et al. (2016); (14) Hogan et al. (2008); (15) Casewell et al. (2014); (16) Lodieu et al. (2014); (17) Lodieu et al. (2019); (18) Schneider et al. (2017); (19) Pérez-Garrido et al. (2017); (20) Bouvier et al. (2008);(20) Liu et al. (2016); (22) Kirkpatrick et al. (2011); (23) Dahn et al. (2017); (24) Kirkpatrick et al. (2016); (25) Chiu et al. (2006); (26) Greco et al. (2019); (27) Lodieu et al. (2009); (28) Marocco et al. (2020); (29) Smart et al. (2013); (30) Mužić et al. (2012).
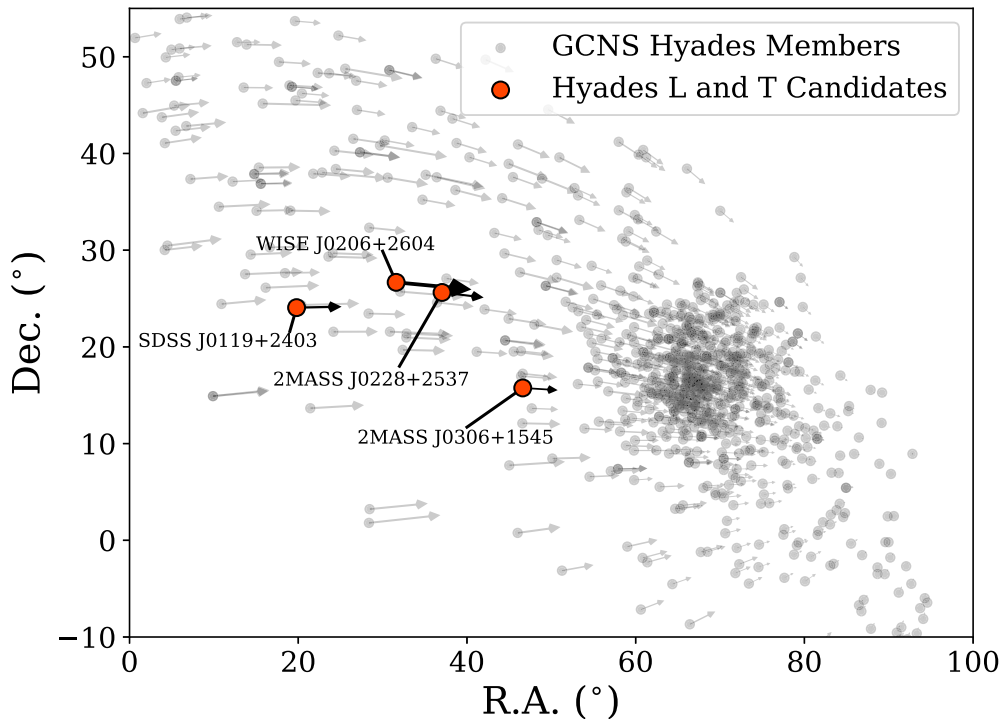
Figure 7. The positions and proper motions of the four new Hyades candidate members identified in this work compared to the list of Hyades members from the Gaia Catalog of Nearby Stars (GCNS; Gaia Collaboration et al. 2021).

following the methods in Hogan et al. (2008), we find a difference between the proper motion angle (θ_μ) and convergent point angle (θ_{cp}) of less than 0°.2 (angles should be similar for true members). We also find a cluster distance (d_c) using the cluster velocity of Lodieu et al. (2019) of 35.9 pc, which is in excellent agreement with the measured distance of 34.6 ± 3.5 pc from Best et al. (2020). We therefore consider SDSS J011912.22+240331.6 to be a new T-type Hyades candidate member.

WISEPA J020625.26+264023.6 was discovered in Kirkpatrick et al. (2011), and was found to be a good match to the L9 standard at J, but much redder at H and K. Liu et al. (2016) reclassified it as L8 (red). We find the same type as Kirkpatrick et al. (2011) in this work (L9 red). Liu et al. (2016) found no matching groups using BANYAN II (Gagné et al. 2014). However, BANYAN II did not include the Hyades and LACEwING has not previously been used for this object to our knowledge. Ashraf et al. (2022) found this object to be a strong variability candidate with a 66.9% probability of belonging to the field, though it is not clear what astrometry was used for this determination. We find a strong Hyades membership probability for this object from LACEwING, with moderate probability from BANYAN Σ. We find a difference between θ_μ and θ_{cp} for this object of ~0°.6. We also find a d_c of 20.0 pc, which agrees well with the measured distance of 19.2 ± 0.5 pc from Liu et al. (2016). We consider WISEPA J020625.26 +264023.6 to be a new substellar candidate Hyades member.

2MASSW J0228110+253738 was discovered in Wilson et al. (2003), with an uncertain near-infrared type of L0. We find a near-infrared spectral type of L1 in this work. This object is returned as a high-probability Hyades member from both BANYAN Σ and LACEwING. Furthermore, there is a radial velocity measurement for this object from Blake et al. (2010; 23.07 ± 0.21 km s^{-1}). Using this radial velocity with the additional astrometry for this object listed in Table 9, we find a

89.1% Hyades membership probability from BANYAN Σ and a 96% membership probability from LACEwING. The difference between θ_μ and θ_{cp} for this object is less than 0°.01, and the d_c of 34.5 pc aligns well with the measured distance of 33.3 ± 0.5 pc from Dahn et al. (2017). We consider 2MASSW J0228110+253738 to be a new candidate Hyades member.

2MASSW J0306268+154514 was discovered in Kirkpatrick et al. (2000) with an optical type of L6:, and we find a near-infrared type of L6.5 in this work. This object was only just omitted by the Hyades study of Schneider et al. (2022), who had a μ_α requirement of $\leqslant 197$ mas yr^{-1} (this object has $\mu_\alpha = 205.4$ mas yr^{-1}). This object just missed the probability threshold of 80% for BANYAN Σ (78.7%) and has a strong Hyades membership probability from LACEwING (98%). This candidate does not have a measured parallax, but the predicted distances from BANYAN Σ (36.4 pc) LACEwING (36.1 pc), and the convergent point (36.7 pc) are all generally consistent with this object's photometric distance estimates (46 ± 8 pc from J, 37 ± 6 pc from K). We consider 2MASSW J0306268 +154514 to be a new Hyades candidate member.

The four new Hyades candidates identified in this work are shown compared to the Hyades member compilation from Gaia Collaboration et al. (2021) in Figure 7. It is clear in the figure that these four candidates exist outside of the cluster center but have motions consistent with known Hyades members. We suggest these four objects as new Hyades cluster candidate members.

5.1.7. The μ Tau Association

The μ Tau Association (MUTA) was first identified in Gagné et al. (2020), with an estimated age of 62 ± 7 Myr. Our search returned a single candidate MUTA member, SIMP J03314657+1944246. This object was discovered in

Robert et al. (2016), who gave a spectral type of L0:: from a very low-S/N near-infrared spectrum. Using UHS proper motions, we find a 97% chance of belonging to MUTA from BANYAN Σ (note that MUTA is not included in LACEwING). The predicted distance if a μ Tau member is $\sim$146 pc, which is not a great match to the photometric distance estimates for this object of 85 ± 14 and 91 ± 15 pc for J- and K-band photometry. However, considering the very uncertain nature of this object's spectral type, it could indeed be a member if it is actual spectral type is earlier than L0. A higher-S/N spectrum of this object would help to clear up potential MUTA membership.

5.1.8. The Taurus Association

Our search recovered one known Taurus member (2MASS J04373705+2331080). Our UHS proper motion is an improvement over previous measurements, and we find a 98.7% chance of belonging to Taurus according to BANYAN Σ (Taurus is not evaluated in LACEwING). This known Taurus member was discovered in Luhman et al. (2009), and is further discussed in Best et al. (2017), Esplin & Luhman (2017), and Kraus et al. (2017).

5.1.9. The 32 Ori Group

The 32 Ori Group (THOR) was first identified in Mamajek (2007) with an age estimate of 15–20 Myr (Luhman 2022). One high-probability THOR member was recovered in our search, i.e., the known member WISE J052857.68+090104.4 (L1 VL-G; Burgasser et al. 2016b). The UHS proper motion of this source is the most precise measurement available, and we find a 99.1% probability of THOR membership from BANYAN Σ and 97.0% probability of THOR membership from LACEwING.

5.1.10. The Ursa Major Association

The Ursa Major Association (UMA) is a loose collection of nearby stars first identified in Eggen (1992) with an estimated age of 414 ± 23 (Jones et al. 2015). Our search returned four previously suggested UMA members and two new candidate members, as summarized in Table 10.

The two new UMA candidates, SDSS J135852.68+374711.9 and PSO J224.3820+47.4057, both have high probabilities of UMA membership from LACEwING using proper motions and parallaxes from Best et al. (2020), but return a 0% probability of UMA membership from BANYAN Σ. We retain both objects as UMA candidate members.

5.1.11. Objects with Ambiguous Membership

The L dwarf 2MASSI J0103320+193536 was once used as the near-infrared L7 standard (Kirkpatrick et al. 2010). However, Faherty et al. (2012) and Allers & Liu (2013) revised the near-infrared spectral type of this object as L6β and L6 INT-G, respectively. Although this object was suggested as a strong Argus candidate member in Gagné et al. (2014), the astrometry used for this source from Faherty et al. (2012) had relatively low precision. Gagné et al. (2015a) again revised the near-infrared type of this object to L6 pec, stating that it showed no clear signs of low-gravity. Faherty et al. (2016) re-evaluated membership and determined its status to be ambiguous. We find similar results in this work using the UHS determined proper motion and a parallax from Kirkpatrick et al. (2021). BANYAN Σ returns a relatively small but not insignificant chance of belonging to Carina-Near (40.7%), while LACEwING suggests Hyades membership (84.0%) and a lower probability of ABDMG membership (56.0%). The membership status of this object remains ambiguous.

5.2. High V_{tan} Objects

Space velocities can be indicative of different populations of the Galaxy. The tangential velocity (V_{tan}) is often used as a rough discriminator between different Galactic components (i.e., thin disk, thick disk, and halo). We have calculated V_{tan} values for every object in our sample, using distances determined from parallaxes or J-band photometry and the most precise proper motions available in an effort to identify previously unknown objects with unusual kinematics.

Nissen (2004) suggest a V_{tan} range for thick-disk objects between 85 and 180 km s^{-1}, with anything over 180 km s^{-1} being a potential halo member. These values are similar to those found in Torres et al. (2019) for the Gaia white dwarf population, who found 90 km s$^{-1} \leqslant V_{tan} \leqslant 200$ km s^{-1} for the thick-disk population and $V_{tan} > 200$ km s^{-1} for the halo (although there is substantial overlap between the different components). We follow the criteria outlined in Dupuy & Liu (2012) to identify objects with a $\geqslant 0.5$ probability of belonging to the thick disk or halo ($V_{tan} > 77 + 35\exp(0.028\ \sigma_{Vtan})$).

Table 11 lists the 13 objects in this sample that were found to have V_{tan} values that satisfy the Dupuy & Liu (2012) criteria. Eleven objects in this sample have measured parallaxes, while the distances to the other two are based on J-band photometry and spectral types. Seven known subdwarfs are recovered in this sample, three of which are newly classified in Table 3 in this work, as well as one "blue" L dwarf.

5.3. Co-moving Companions

Co-moving L, T, and Y type companions serve as valuable benchmarks for tests of stellar and substellar models (e.g., Faherty et al. 2010; Deacon et al. 2014). We have cross-matched our sample against Gaia DR3 Gaia Collaboration et al. (2023) to identify any primary components of previously unrecognized multiple systems. This search returned seven new wide multiple systems containing at least one member with a spectral type of L0 or later. We evaluated each newly identified system with the COMOVER (Gagné et al. 2021) tool. Photometric distances were used in COMOVER when parallactic distances were not available. The new systems identified in this work and their co-moving probabilities according to COMOVER are listed in Table 12.

For SDSS J081132.87+485532.9 (L0; Kiman et al. 2019), we find a white dwarf co-moving companion in Gaia, with a separation of $\sim$2″. The UHS proper motion of SDSS J081132.87+485532.9 matches well with the white dwarf, but the distance from the white dwarf parallax (196.53 ± 26.52; Gaia Collaboration et al. 2023) does not match the J-band photometric distance of SDSS J081132.87+485532.9 (106 ± 18 pc). It is possible that the spectral type of SDSS J081132.87+485532.9 determined in Kiman et al. (2019) is inaccurate, and this is instead an M-type companion to a white dwarf at $\sim$200 pc.

Table 10
Ursa Major Members and Candidate Members

Name	Sp. Type	References	μ_α (mas yr^{-1})	μ_δ (mas yr^{-1})	References	ϖ (mas)	References	BANYAN (%)	LACEwING (%)	References[a]
Recovered Members										
WISEA J120104.57+573004.2	L9	1	99.0 ± 3.5	13.2 ± 3.6	2	[28 ± 5]	2	91.1	0.0	3
2MASSW J1239272+551537	L5	4	125.2 ± 1.1	−0.4 ± 1.1	5	42.4 ± 2.1	5	94.1	100.0	6
2MASSW J1246467+402715	L5	2	129.57 ± 0.47	−103.97 ± 0.46	7	44.74 ± 0.63	7	0.0	98.0	6,8
SDSS J125011.65+392553.9	T4	9	−42.4 ± 3.4	−830.5 ± 2.6	10	42.8 ± 3.2	10	0.0	100.0	11
New Candidate Members										
SDSS J135852.68+374711.9	T5	12	−27.0 ± 2.8	−455.7 ± 2.5	10	49.6 ± 3.1	10	0.0	100.0	...
PSO J224.3820+47.4057	T7	13	140.0 ± 3.0	−84.7 ± 2.3	10	49.5 ± 2.9	10	0.0	99.0	...

Note.
[a] References in the final column are the relevant works that have previously evaluated, suggested, or determined moving group membership.

References. (1) Schneider et al. (2017); (2) This work; (3) Ashraf et al. (2022); (4) Schneider et al. (2014); (5) Dupuy & Liu (2012); (6) Jameson et al. (2008); (7) Gaia Collaboration et al. (2023); (8) Ujjwal et al. (2020); (9) Chiu et al. (2006); (10) Best et al. (2020); (11) Zhang et al. (2021); (12) Burgasser et al. (2010); (13) Best et al. (2015).

Table 11
High $V_{\rm tan}$ Objects

Name	Spectral Type	References	Dist.[a] (pc)	References	$\mu_{\rm tot}$ (mas yr^{-1})	References	$V_{\rm tan}$[a] (km s^{-1})
WISEA J004326.26+222124.0	sdL1	1	66.71 ± 1.30	2	441.33 ± 0.18	2	139.6 ± 2.7
WISEA J030845.36+325923.1	sdL1	3	53.77 ± 4.13	2	493.09 ± 1.09	2	125.7 ± 9.7
SDSS J033456.32+010618.7	L0.5	4	[116 ± 20]	3	401.68 ± 5.22	4	[220 ± 38]
WISEA J043535.82+211508.9	sdL0	1	59.71 ± 2.12	2	1288.77 ± 0.39	2	364.8 ± 12.9
SDSS J100016.92+321829.4	L1	5	[69 ± 12]	3	487.45 ± 3.71	6	[159 ± 28]
SDSS J103143.09+524558.7	L0	7	76.89 ± 4.59	2	349.53 ± 0.47	2	127.4 ± 7.6
SDSS J125045.66+441853.7	L0	8	136.20 ± 15.03	2	284.68 ± 0.45	2	183.8 ± 20.3
2MASSW J1411175+393636	L1.5	9	29.65 ± 0.39	2	930.68 ± 0.24	2	130.8 ± 1.7
2MASS J14343616+2202463	d/sdL1	3	31.64 ± 0.80	2	770.25 ± 0.35	2	115.5 ± 2.9
2MASS J16262034+3925190	sdL4	10	30.93 ± 0.14	2	1395.11 ± 0.11	2	204.5 ± 0.9
2MASS J16403197+1231068	sdL0:	3	101.81 ± 4.30	2	260.60 ± 0.24	2	125.8 ± 5.3
2MASSI J1721039+334415	L3 (blue)	3	16.18 ± 0.04	2	1947.39 ± 0.11	2	149.4 ± 0.4
2MASS J17561080+2815238	sdL1	10	34.56 ± 0.32	2	740.78 ± 0.19	2	121.3 ± 1.1

Note.
[a] Distances listed in square brackets are photometric J-band distances using Table 5. Likewise, $V_{\rm tan}$ values given in square brackets are derived from these distances.
References. (1) Kirkpatrick et al. (2014); (2) Gaia Collaboration et al. (2023); (3) This work.; (4) Scholz et al. (2009); (5) Schmidt et al. (2010); (6) Best et al. (2018); (7) Kiman et al. (2019); (8) West et al. (2008); (9) Bardalez Gagliuffi et al. (2014); (10) Greco et al. (2019).

6. Summary

We have presented photometry and astrometry for all spectroscopically confirmed L, T, and Y dwarfs in the UKIRT Hemisphere Survey. We have determined typical colors and absolute magnitudes using UHS photometry for normal L, T, and Y dwarfs. We have also determined proper motions for each object detected in both the UHS J- and K-band surveys (768 total), 381 of which are the most precise proper motions yet measured.

Using the best available astrometry for each object, we have strengthened the membership status for several previously suggested moving group members and identified 16 new candidate members. We have further identified a number of high tangential-velocity objects and seven previously overlooked wide-separation L-type co-moving companions.

Transforming UHS positions to the Gaia reference frame vastly improved their accuracy and precision. Similar improvements could be applied to other previous publicly available surveys. For example, astrometric calibrations for all previous UKIDSS surveys were performed using the 2MASS point-source catalog (Dye et al. 2006), which is itself tied to the Tycho astrometric calibration (Høg et al. 2000). Astrometric calibrations for all VISTA surveys (McMahon et al. 2013) are also performed using the 2MASS point-source catalog.[6] Re-registering these surveys would allow for new, more accurate, and precise proper motion investigations, and would produce an astrometric catalog with similar near-infrared depths between declinations of −90° to +60°, with only the north celestial pole yet to be surveyed.

Acknowledgments

---

6 https://www.eso.org/rm/api/v1/public/releaseDescriptions/144

Table 12
New Co-moving Companions

Name	Sp. Type	References	μ_α (mas yr^{-1})	μ_δ (mas yr^{-1})	References	Dist.[a] (pc)	References	Sep. ($''$)	COMOVER (%)
SDSS J075259.47+413646.7	M7	1	-23.21 ± 0.18	10.64 ± 0.15	2	85.22 ± 1.15	2	...	...
SDSS J075259.43+413634.6	L0	3	-21.7 ± 2.2	10.1 ± 2.3	4	$[95 \pm 16]$	4	12.0	99.98
Gaia DR3 931634554610889728	WD	5	9.26 ± 0.56	-47.68 ± 0.51	2	196.53 ± 26.52	2	...	...
SDSS J081132.87+485532.9	L0	6	7.8 ± 3.2	-45.8 ± 2.6	4	$[106 \pm 18]$	4	2.3	93.68
TYC 813-243-1A	K5	7	-41.75 ± 0.02	-70.55 ± 0.01	2	64.87 ± 0.08	2	...	...
TYC 813-243-1B	...	...	-39.19 ± 0.02	-71.83 ± 0.02	2	64.92 ± 0.10	2	1.9	...
SDSS J084457.38+120825.4	L0	6	-39.85 ± 0.48	-70.61 ± 0.34	2	65.90 ± 1.79	2	55.5	100.00
HD 76945	F2	8	-95.66 ± 0.06	-26.86 ± 0.06	2	75.13 ± 0.35	2	...	...
PSO J135.0395+32.0845	L1.5	9	-97.25 ± 1.57	-25.08 ± 1.37	2	69.52 ± 5.92	2	61.2	100.00
LSPM J1230+4048	M3	11	-155.15 ± 0.02	32.16 ± 0.02	2	62.50 ± 0.09	2	...	...
SDSS J123112.97+405027.9	L0	10	-156.27 ± 0.35	31.53 ± 0.45	2	60.93 ± 1.82	2	187.4	100.00
ATO J199.1400+57.6089	M4	11	43.12 ± 0.09	19.70 ± 0.09	2	48.08 ± 0.22	2	...	...
SDSS J131633.79+573549.1	L0	6	48.52 ± 0.21	17.49 ± 0.20	2	48.30 ± 0.47	2	43.0	100.00
Gaia DR3 2816131994957537280	...	...	38.29 ± 0.11	-13.06 ± 0.09	2	96.53 ± 0.97	2	...	...
SDSS J230134.21+144219.6	L0	6	42.3 ± 3.2	-12.51 ± 4.0	4	$[90 \pm 15]$	4	52.5	99.99

Note.
[a] Distances listed in square brackets are *J*-band photometric distances derived using the relation derived in Section 3.

References. (1) West et al. (2011); (2) Gaia Collaboration et al. (2023); (3) Hawley et al. (2002); (4) This work; (5) Gentile Fusillo et al. (2019); (6) Kiman et al. (2019); (7) Pickles & Depagne (2010); (8) Cannon & Pickering (1919); (9) Best et al. (2015); (10) Schmidt et al. (2010); (11) Luo et al. (2015).

Appendix
The UHS L, T, and Y Dwarf Catalog

The following table includes the astrometry and photometry for all of the known L, T, and Y dwarfs in the UHS survey.

Table A1
Sample Properties

Column Label	Description	Example	Units
Disc_Name	Discovery name	SDSS J000013.54+255418.6	...
Disc_ref	Discovery reference	1	...
SpT_Opt	Optical spectral type	T5	...
SpT_Opt_ref	Reference for optical spectral type	111	...
SpT_IR	Near-infrared spectral type	T4.5	...
SpT_IR_ref	Reference for near-infrared spectral type	1	...
RA_UHS	UHS DR2 R.A.	0.0563546	degrees
Dec_UHS	UHS DR2 decl.	25.9055694	degrees
RA_UHS_J	UHS J-band R.A.	0.0564025	degrees
eRA_UHS_J	Uncertainty of UHS J-band R.A.	15.10	mas
Dec_UHS_J	UHS J-band decl.	25.9055032	degrees
eDec_UHS_J	Uncertainty of UHS J-band decl.	12.13	mas
UHS_J_epoch	UHS J-band epoch	2013.484	years
RA_UHS_K	UHS K-band R.A.	0.5635380	degrees
eRA_UHS_K	Uncertainty of UHS K-band R.A.	10.29	mas
Dec_UHS_K	UHS K-band decl.	25.9056502	degrees
eDec_UHS_K	Uncertainty of UHS K-band decl.	10.76	mas
UHS_K_epoch	UHS K-band epoch	2017.749	years
Jmag	UHS J magnitude	14.8459	mag
eJmag	Uncertainty of UHS J magnitude	0.0049	mag
Kmag	UHS K magnitude	14.9702	mag
eKmag	Uncertainty of UHS K magnitude	0.0164	mag
UHS_pmra	UHS μ_α	−26.68	mas yr^{-1}
UHS_epmra	UHS uncertainty of μ_α	2.25	mas yr^{-1}
UHS_pmdec	UHS μ_δ	127.84	mas yr^{-1}
UHS_epmdec	UHS uncertainty of μ_δ	2.35	mas yr^{-1}
RA_Gaia	Gaia DR3 R.A.	0.05635442742	degrees
Dec_Gaia	Gaia DR3 decl.	25.90556949064	degrees
Gaia_plx	Parallax from Gaia DR3	...	mas
Gaia_eplx	Uncertainty of Gaia DR3 parallax	...	mas
Gaia_pmra	Gaia DR3 μ_α	...	mas yr^{-1}
Gaia_epmra	Gaia DR3 uncertainty of μ_α	...	mas yr^{-1}
Gaia_pmdec	Gaia DR3 μ_δ	...	mas yr^{-1}
Gaia_epmdec	Gaia DR3 uncertainty of μ_δ	...	mas yr^{-1}
Gmag	Gaia DR3 G magnitude	21.380291	mag
RPmag	Gaia DR3 G$_{RP}$ magnitude	19.64465	mag
BPmag	Gaia DR3 G$_{BP}$ magnitude	...	mag
Name_PS1	Pan-Starrs DR2 designation	PSO J000.0564+25.9054	...
RA_PS1	Pan-Starrs DR2 R.A.	0.05638003	degrees
Dec_PS1	Pan-Starrs DR2 decl.	25.90545405	degrees
gmag	Pan-Starrs g magnitude	...	mag
egmag	Pan-Starrs g uncertainty	...	mag
rmag	Pan-Starrs r magnitude	...	mag
ermag	Pan-Starrs r uncertainty	...	mag
imag	Pan-Starrs i magnitude	...	mag
eimag	Pan-Starrs i uncertainty	...	mag
zmag	Pan-Starrs z magnitude	19.1981	mag
ezmag	Pan-Starrs z uncertainty	0.0152	mag
ymag	Pan-Starrs y magnitude	17.4245	mag
eymag	Pan-Starrs y uncertainty	0.0083	mag
PS1_pmra	Best et al. (2018) μ_α	−18.4	mas yr^{-1}
PS1_epmra	Best et al. (2018) uncertainty of μ_α	5.5	mas yr^{-1}
PS1_pmdec	Best et al. (2018) μ_δ	123.1	mas yr^{-1}
PS1_epmdec	Best et al. (2018) uncertainty of μ_δ	3.3	mas yr^{-1}
Name_CWISE	CatWISE 2020 designation	J000013.51+255419.7	...
RA_CWISE	CatWISE 2020 R.A.	0.0563043	degrees
Dec_CWISE	CatWISE 2020 decl.	25.9054854	degrees
W1	CatWISE 2020 W1 magnitude	12.922	mag
eW1	CatWISE 2020 W1 magnitude uncertainty	0.017	mag
W2	CatWISE 2020 W2 magnitude	12.155	mag
eW2	CatWISE 2020 W2 magnitude uncertainty	0.010	mag
CWISE_pmra	CatWISE 2020 μ_α	−20.31	mas yr^{-1}
CWISE_epmra	CatWISE 2020 uncertainty of μ_α	6.4	mas yr^{-1}

Table A1
(Continued)

Column Label	Description	Example	Units
CWISE_pmdec	CatWISE 2020 μ_δ	50.97	mas yr^{-1}
CWISE_epmdec	CatWISE 2020 uncertainty of μ_δ	6.3	mas yr^{-1}
O_pmra	Optimal μ_α	−19.09	mas yr^{-1}
O_epmra	Uncertainty of optimal μ_α	1.44	mas yr^{-1}
O_pmdec	Optimal μ_δ	126.67	mas yr^{-1}
O_epmdec	Uncertainty of optimal μ_δ	1.30	mas yr^{-1}
pm_ref	Reference for optimal proper motion	132	...
O_plx	Optimal parallax	70.8	mas
O_eplx	Uncertainty of optimal parallax	1.9	mas
plx_ref	Reference for optimal parallax	132	...
flag	flag[a]	10,14	...

Note.

[a] Flags: 1 = young or suggested to be young; 2 = subdwarf; 3 = visual binary; 4 = Hyades member or candidate member; 5 = red near-infrared spectrum; 6 = spectral binary; 7 = wide companion; 8 = peculiar spectrum; 9 = uncertain spectral type; 10 = poor or contaminated CatWISE 2020 photometry; 11 = poor or contaminated Pan-STARRS photometry; 12 = blue near-infrared spectrum; 13 = Gaia RUWE $\geqslant$ 1.4; 14 = photometry from CatWISE 2020 reject catalog; 15 = Parallax given is from co-moving companion; 16 = UHS photometry near saturation limit.

References. (1) Knapp et al. (2004); (2) Chiu et al. (2006); (3) Mace et al. (2013); (4) Zhang et al. (2010); (5) Schneider et al. (2016); (6) Kirkpatrick et al. (2010); (7) Kellogg et al. (2017); (8) Kirkpatrick et al. (2000); (9) Best et al. (2015); (10) Best et al. (2020); (11) Aller et al. (2016); (12) Zhang et al. (2019); (13) Reid et al. (2006); (14) Burgasser et al. (2010); (15) Deacon et al. (2014); (16) Kirkpatrick et al. (1999); (17) Thompson et al. (2013); (18) Reid et al. (2000); (19) Mugrauer et al. (2006); (20) Burgasser et al. (2004); (21) Luhman (2014); (22) Wilson et al. (2003); (23) Meisner et al. (2020b); (24) Naud et al. (2014); (25) Kirkpatrick et al. (2011); (26) Cruz et al. (2007); (27) Kirkpatrick et al. (2012); (28) Robert et al. (2016); (29) Schneider et al. (2017); (30) Day-Jones et al. (2013); (31) Hawley et al. (2002); (32) Schmidt et al. (2010); (33) Deacon et al. (2017); (34) Cruz et al. (2003); (35) Albert et al. (2011); (36) Scholz et al. (2011); (37) Lodieu et al. (2009); (38) Luhman & Sheppard (2014); (39) Schneider et al. (2022); (40) Marocco et al. (2015); (41) West et al. (2008); (42) Gizis et al. (2003); (43) West et al. (2011); (44) Vos et al. (2022); (45) Zhang et al. (2020); (46) Reid et al. (2008); (47) Cushing et al. (2011); (48) Hogan et al. (2008); (49) Pérez-Garrido et al. (2017); (50) Luhman (2006); (51) Pérez-Garrido et al. (2018); (52) Bouvier et al. (2008); (53) Luhman et al. (2009); (54) Schneider et al. (2023); (55) Bihain et al. (2013); (56) Looper et al. (2007); (57) Lépine et al. (2002); (58) Kirkpatrick et al. (2021); (59) Mužić et al. (2012); (60) Best et al. (2013); (61) Kirkpatrick et al. (2014);(62) Thorstensen & Kirkpatrick (2003); (63) Burgasser et al. (2002); (64) Kiman et al. (2019); (65) Zhang et al. (2009); (66) Skrzypek et al. (2016); (67) Reylé (2018); (68) Smith et al. (2014); (69) Schmidt et al. (2015); (70) Scholz (2010); (71) Aberasturi et al. (2011); (72) Geballe et al. (2002); (73) Deacon et al. (2009); (74) Bouy et al. (2003); (75) Reylé et al. (2010); (76) Wilson et al. (2001); (77) Burningham et al. (2013); (78) Cushing et al. (2014); (79) Tinney (1993); (80) Sheppard & Cushing (2009); (81) Rebolo et al. (1998); (82) Baron et al. (2015); (83) Schmidt et al. (2007); (84) Burgasser et al. (1999); (85) Kuchner et al. (2017); (86) Wright et al. (2013); (87) Kellogg et al. (2015); (88) Gizis et al. (2000); (89) Deacon et al. (2011); (90) Stern et al. (2007); (91) Burgasser et al. (2003c); (92) Faherty et al. (2009); (93) Metchev et al. (2008); (94) Kirkpatrick et al. (2016); (95) Burgasser et al. (2011); (96) Artigau et al. (2011);(97) Strauss et al. (1999); (98) Bardalez Gagliuffi et al. (2014); (99) Schneider et al. (2002); (100) Radigan et al. (2008); (101) Gizis et al. (2011a); (102) Marocco et al. (2020); (103) Luhman et al. (2012); (104) Looper et al. (2008); (105) Jameson et al. (2008); (106) Gizis et al. (2011b); (107) Burgasser et al. (2006a); (108) Luhman et al. (2007); (109) Martin et al. (2018); (110) Dahn et al. (2002); (111) Pineda et al. (2016); (112) Zhang et al. (2017); (113) Cruz et al. (2009); (114) Scholz et al. (2009); (115) Lodieu et al. (2014); (116) Burgasser et al. (2003b); (117) Faherty et al. (2013); (118) Burgasser (2007); (119) Cruz et al. (2018); (120) Gizis et al. (2015); (121) Gizis et al. (2013); (122) Kirkpatrick et al. (2008); (123) This work; (124) Schneider et al. (2014); (125) Allers & Liu (2013); (126) Dupuy et al. (2015); (127) Greco et al. (2019); (128) Liu et al. (2011); (129) Gagné et al. (2015a); (130) Liu et al. (2016); (131) Best et al. (2017); (132) Dupuy & Liu (2012);(133) Bouy et al. (2004); (134) Radigan et al. (2013); (135) Faherty et al. (2016); (136) Leggett et al. (2014); (137) Bardalez Gagliuffi et al. (2019); (138) Gaia Collaboration et al. (2023); (139) Best et al. (2018); (140) Dahn et al. (2017); (141) Kirkpatrick et al. (2019); (142) Marocco et al. (2021); (143) Lodieu et al. (2019); (144) Meisner et al. (2020a); (145) Gaia Collaboration et al. (2018); (146) Schilbach et al. (2009); (147) Vrba et al. (2004); (148) Tinney et al. (2003); (149) Sahlmann et al. (2016); (150) Zhang et al. (2021); (151) Smart et al. (2013); (152) van Leeuwen (2007); (153) Zapatero Osorio et al. (2014); (154) Manjavacas et al. (2013); (155) Dupuy & Liu (2017); (156) Burgasser (2004); (157) Burgasser et al. (2016b).

(This table is available in its entirety in machine-readable form.)

ORCID iDs

Adam C. Schneider ● https://orcid.org/0000-0002-6294-5937
Jeffrey A. Munn ● https://orcid.org/0000-0002-4603-4834
Justice Bruursema ● https://orcid.org/0000-0002-3858-1205
Scott E. Dahm ● https://orcid.org/0000-0002-2968-2418
Michael C. Liu ● https://orcid.org/0000-0003-2232-7664
Bryan N. Dorland ● https://orcid.org/0000-0002-5604-5254

References

Aberasturi, M., Solano, E., & Martín, E. L. 2011, A&A, 534, L7
Albert, L., Artigau, É., Delorme, P., et al. 2011, AJ, 141, 203
Aller, K. M., Liu, M. C., Magnier, E. A., et al. 2016, ApJ, 821, 120
Allers, K. N., & Liu, M. C. 2013, ApJ, 772, 79
Artigau, É., Lafrenière, D., Doyon, R., et al. 2011, ApJ, 739, 48

Ashraf, A., Bardalez Gagliuffi, D. C., Manjavacas, E., et al. 2022, ApJ, 934, 178
Bardalez Gagliuffi, D. C., Burgasser, A. J., Gelino, C. R., et al. 2014, ApJ, 794, 143
Bardalez Gagliuffi, D. C., Burgasser, A. J., Schmidt, S. J., et al. 2019, ApJ, 883, 205
Baron, F., Lafrenière, D., Artigau, É., et al. 2015, ApJ, 802, 37
Bell, C. P. M., Mamajek, E. E., & Naylor, T. 2015, MNRAS, 454, 593
Best, W. M. J., Liu, M. C., Magnier, E. A., et al. 2013, ApJ, 777, 84
Best, W. M. J., Liu, M. C., Magnier, E. A., et al. 2015, ApJ, 814, 118
Best, W. M. J., Liu, M. C., Magnier, E. A., et al. 2017, ApJ, 837, 95
Best, W. M. J., Liu, M. C., Magnier, E. A., et al. 2020, AJ, 159, 257
Best, W. M. J., Liu, M. C., Magnier, E. A., et al. 2021, AJ, 161, 42
Best, W. M. J., Magnier, E. A., Liu, M. C., et al. 2018, ApJS, 234, 1
Bihain, G., Scholz, R.-D., Storm, J., et al. 2013, A&A, 557, A43
Blake, C. H., Charbonneau, D., & White, R. J. 2010, ApJ, 723, 684
Bouvier, J., Kendall, T., Meeus, G., et al. 2008, A&A, 481, 661
Bouy, H., Brandner, W., Martín, E. L., et al. 2003, AJ, 126, 1526
Bouy, H., Duchêne, G., Köhler, R., et al. 2004, A&A, 423, 341

Burgasser, A. J. 2004, ApJL, 614, L73
Burgasser, A. J. 2007, AJ, 134, 1330
Burgasser, A. J. & Splat Development Team 2017, in ASI Conf. Ser. 14, 3rd Int. Workshop on Spectral Stellar Libraries, ed. P. Coelho et al. (Hyderabad: ASI), 7
Burgasser, A. J., Blake, C. H., Gelino, C. R., et al. 2016a, ApJ, 827, 25
Burgasser, A. J., Cruz, K. L., Cushing, M., et al. 2010, ApJ, 710, 1142
Burgasser, A. J., Cushing, M. C., Kirkpatrick, J. D., et al. 2011, ApJ, 735, 116
Burgasser, A. J., Dhital, S., & West, A. A. 2009, AJ, 138, 1563
Burgasser, A. J., Geballe, T. R., Leggett, S. K., et al. 2006a, ApJ, 637, 1067
Burgasser, A. J., Kirkpatrick, J. D., Brown, M. E., et al. 1999, ApJL, 522, L65
Burgasser, A. J., Kirkpatrick, J. D., Brown, M. E., et al. 2002, ApJ, 564, 421
Burgasser, A. J., Kirkpatrick, J. D., Burrows, A., et al. 2003a, ApJ, 592, 1186
Burgasser, A. J., Kirkpatrick, J. D., Cruz, K. L., et al. 2006b, ApJS, 166, 585
Burgasser, A. J., Kirkpatrick, J. D., Liebert, J., et al. 2003b, ApJ, 594, 510
Burgasser, A. J., Kirkpatrick, J. D., & Lowrance, P. J. 2005, AJ, 129, 2849
Burgasser, A. J., Kirkpatrick, J. D., McElwain, M. W., et al. 2003c, AJ, 125, 850
Burgasser, A. J., Lopez, M. A., Mamajek, E. E., et al. 2016b, ApJ, 820, 32
Burgasser, A. J., McElwain, M. W., Kirkpatrick, J. D., et al. 2004, AJ, 127, 2856
Burningham, B., Cardoso, C. V., Smith, L., et al. 2013, MNRAS, 433, 457
Cannon, A. J., & Pickering, E. C. 1919, AnHar, 94, 1
Casali, M., Adamson, A., Alves de Oliveira, C., et al. 2007, A&A, 467, 777
Casewell, S. L., Littlefair, S. P., Burleigh, M. R., et al. 2014, MNRAS, 441, 2644
Chambers, K. C., Magnier, E. A., Metcalfe, N., et al. 2016, arXiv:1612.05560
Chiu, K., Fan, X., Leggett, S. K., et al. 2006, AJ, 131, 2722
Couture, D., Gagné, J., & Doyon, R. 2023, ApJ, 946, 6
Cruz, K. L., Kirkpatrick, J. D., & Burgasser, A. J. 2009, AJ, 137, 3345
Cruz, K. L., Núñez, A., Burgasser, A. J., et al. 2018, AJ, 155, 34
Cruz, K. L., Reid, I. N., Kirkpatrick, J. D., et al. 2007, AJ, 133, 439
Cruz, K. L., Reid, I. N., Liebert, J., et al. 2003, AJ, 126, 2421
Cushing, M. C., Kirkpatrick, J. D., Gelino, C. R., et al. 2011, ApJ, 743, 50
Cushing, M. C., Kirkpatrick, J. D., Gelino, C. R., et al. 2014, AJ, 147, 113
Cushing, M. C., Saumon, D., & Marley, M. S. 2010, AJ, 140, 1428
Dahn, C. C., Harris, H. C., Subasavage, J. P., et al. 2017, AJ, 154, 147
Dahn, C. C., Harris, H. C., Vrba, F. J., et al. 2002, AJ, 124, 1170
Day-Jones, A. C., Marocco, F., Pinfield, D. J., et al. 2013, MNRAS, 430, 1171
Deacon, N. R., Hambly, N. C., King, R. R., et al. 2009, MNRAS, 394, 857
Deacon, N. R., Liu, M. C., Magnier, E. A., et al. 2011, AJ, 142, 77
Deacon, N. R., Liu, M. C., Magnier, E. A., et al. 2014, ApJ, 792, 119
Deacon, N. R., Magnier, E. A., Liu, M. C., et al. 2017, MNRAS, 467, 1126
Dupuy, T. J., & Kraus, A. L. 2013, Sci, 341, 1492
Dupuy, T. J., & Liu, M. C. 2012, ApJS, 201, 19
Dupuy, T. J., & Liu, M. C. 2017, ApJS, 231, 15
Dupuy, T. J., Liu, M. C., & Leggett, S. K. 2015, ApJ, 803, 102
Dye, S., Lawrence, A., Read, M. A., et al. 2018, MNRAS, 473, 5113
Dye, S., Warren, S. J., Hambly, N. C., et al. 2006, MNRAS, 372, 1227
Eggen, O. J. 1992, AJ, 104, 1493
Epchtein, N., de Batz, B., Capoani, L., et al. 1997, Msngr, 87, 27
Esplin, T. L., & Luhman, K. L. 2017, AJ, 154, 134
Faherty, J. K., Burgasser, A. J., Cruz, K. L., et al. 2009, AJ, 137, 1
Faherty, J. K., Burgasser, A. J., Walter, F. M., et al. 2012, ApJ, 752, 56
Faherty, J. K., Burgasser, A. J., West, A. A., et al. 2010, AJ, 139, 176
Faherty, J. K., Gagné, J., Popinchalk, M., et al. 2021, ApJ, 923, 48
Faherty, J. K., Goodman, S., Caselden, D., et al. 2020, ApJ, 889, 176
Faherty, J. K., Rice, E. L., Cruz, K. L., et al. 2013, AJ, 145, 2
Faherty, J. K., Riedel, A. R., Cruz, K. L., et al. 2016, ApJS, 225, 10
Gagné, J., David, T. J., Mamajek, E. E., et al. 2020, ApJ, 903, 96
Gagné, J., & Faherty, J. K. 2018, ApJ, 862, 138
Gagné, J., Faherty, J. K., Cruz, K. L., et al. 2015a, ApJS, 219, 33
Gagné, J., Faherty, J. K., Schneider, A. C., et al. 2021, CoMover: Bayesian probability of co-moving stars, Astrophysics Source Code Library, ascl:2106.007
Gagné, J., Lafrenière, D., Doyon, R., et al. 2014, ApJ, 783, 121
Gagné, J., Lafrenière, D., Doyon, R., et al. 2015b, ApJ, 798, 73
Gagné, J., Mamajek, E. E., Malo, L., et al. 2018, ApJ, 856, 23
Gaia Collaboration, Brown, A. G. A., Vallenari, A., et al. 2018, A&A, 616, A1
Gaia Collaboration, Smart, R. L., Sarro, L. M., et al. 2021, A&A, 649, A6
Gaia Collaboration, Vallenari, A., Brown, A. G. A., et al. 2023, A&A, 674, A1
Geballe, T. R., Knapp, G. R., Leggett, S. K., et al. 2002, ApJ, 564, 466
Geißler, K., Metchev, S., Kirkpatrick, J. D., et al. 2011, ApJ, 732, 56
Gentile Fusillo, N. P., Tremblay, P.-E., Gänsicke, B. T., et al. 2019, MNRAS, 482, 4570
Gizis, J. E., Burgasser, A. J., Berger, E., et al. 2013, ApJ, 779, 172

Gizis, J. E., Burgasser, A. J., Faherty, J. K., et al. 2011a, AJ, 142, 171
Gizis, J. E., Burgasser, A. J., & Vrba, F. J. 2015, AJ, 150, 179
Gizis, J. E., Monet, D. G., Reid, I. N., et al. 2000, AJ, 120, 1085
Gizis, J. E., Reid, I. N., Knapp, G. R., et al. 2003, AJ, 125, 3302
Gizis, J. E., Troup, N. W., & Burgasser, A. J. 2011b, ApJL, 736, L34
Greco, J. J., Schneider, A. C., Cushing, M. C., et al. 2019, AJ, 158, 182
Hawley, S. L., Covey, K. R., Knapp, G. R., et al. 2002, AJ, 123, 3409
Hiranaka, K., Cruz, K. L., Douglas, S. T., et al. 2016, ApJ, 830, 96
Hodgkin, S. T., Irwin, M. J., Hewett, P. C., et al. 2009, MNRAS, 394, 675
Høg, E., Fabricius, C., Makarov, V. V., et al. 2000, A&A, 355, L27
Hogan, E., Jameson, R. F., Casewell, S. L., et al. 2008, MNRAS, 388, 495
Hsu, C.-C., Burgasser, A. J., Theissen, C. A., et al. 2021, ApJS, 257, 45
Jameson, R. F., Casewell, S. L., Bannister, N. P., et al. 2008, MNRAS, 384, 1399
Jones, J., White, R. J., Boyajian, T., et al. 2015, ApJ, 813, 58
Kaiser, N., Burgett, W., Chambers, K., et al. 2010, Proc. SPIE, 7733, 77330E
Kellogg, K., Metchev, S., Geißler, K., et al. 2015, AJ, 150, 182
Kellogg, K., Metchev, S., Miles-Páez, P. A., et al. 2017, AJ, 154, 112
Kiman, R., Schmidt, S. J., Angus, R., et al. 2019, AJ, 157, 231
Kirkpatrick, J. D. 2005, ARA&A, 43, 195
Kirkpatrick, J. D., Cruz, K. L., Barman, T. S., et al. 2008, ApJ, 689, 1295
Kirkpatrick, J. D., Cushing, M. C., Gelino, C. R., et al. 2011, ApJS, 197, 19
Kirkpatrick, J. D., Gelino, C. R., Cushing, M. C., et al. 2012, ApJ, 753, 156
Kirkpatrick, J. D., Gelino, C. R., Faherty, J. K., et al. 2021, ApJS, 253, 7
Kirkpatrick, J. D., Kellogg, K., Schneider, A. C., et al. 2016, ApJS, 224, 36
Kirkpatrick, J. D., Looper, D. L., Burgasser, A. J., et al. 2010, ApJS, 190, 100
Kirkpatrick, J. D., Martin, E. C., Smart, R. L., et al. 2019, ApJS, 240, 19
Kirkpatrick, J. D., Reid, I. N., Liebert, J., et al. 1999, ApJ, 519, 802
Kirkpatrick, J. D., Reid, I. N., Liebert, J., et al. 2000, AJ, 120, 447
Kirkpatrick, J. D., Schneider, A., Fajardo-Acosta, S., et al. 2014, ApJ, 783, 122
Kiwy, F., Faherty, J. K., Meisner, A., et al. 2022, AJ, 164, 3
Knapp, G. R., Leggett, S. K., Fan, X., et al. 2004, AJ, 127, 3553
Kraus, A. L., Herczeg, G. J., Rizzuto, A. C., et al. 2017, ApJ, 838, 150
Kuchner, M. J., Faherty, J. K., Schneider, A. C., et al. 2017, ApJL, 841, L19
Law, N. M., Dhital, S., Kraus, A., et al. 2010, ApJ, 720, 1727
Leggett, S. K., Liu, M. C., Dupuy, T. J., et al. 2014, ApJ, 780, 62
Lépine, S., Shara, M. M., & Rich, R. M. 2002, AJ, 124, 1190
Lindegren, L., Hernández, J., Bombrun, A., et al. 2018, A&A, 616, A2
Linsky, J. L. 1969, ApJ, 156, 989
Liu, M. C., Deacon, N. R., Magnier, E. A., et al. 2011, ApJL, 740, L32
Liu, M. C., Dupuy, T. J., & Allers, K. N. 2013, AN, 334, 85
Liu, M. C., Dupuy, T. J., & Allers, K. N. 2016, ApJ, 833, 96
Liu, M. C., Dupuy, T. J., Bowler, B. P., et al. 2012, ApJ, 758, 57
Liu, M. C., Leggett, S. K., Golimowski, D. A., et al. 2006, ApJ, 647, 1393
Lodieu, N., Boudreault, S., & Béjar, V. J. S. 2014, MNRAS, 445, 3908
Lodieu, N., Burningham, B., Hambly, N. C., et al. 2009, MNRAS, 397, 258
Lodieu, N., Smart, R. L., Pérez-Garrido, A., et al. 2019, A&A, 623, A35
Looper, D. L., Kirkpatrick, J. D., & Burgasser, A. J. 2007, AJ, 134, 1162
Looper, D. L., Kirkpatrick, J. D., Cutri, R. M., et al. 2008, ApJ, 686, 528
Luhman, K. L. 2006, ApJ, 645, 676
Luhman, K. L. 2014, ApJ, 781, 4
Luhman, K. L. 2022, AJ, 164, 151
Luhman, K. L., Loutrel, N. P., McCurdy, N. S., et al. 2012, ApJ, 760, 152
Luhman, K. L., Mamajek, E. E., Allen, P. R., et al. 2009, ApJ, 703, 399
Luhman, K. L., Patten, B. M., Marengo, M., et al. 2007, ApJ, 654, 570
Luhman, K. L., & Sheppard, S. S. 2014, ApJ, 787, 126
Luo, A.-L., Zhao, Y.-H., Zhao, G., et al. 2015, RAA, 15, 1095
Mace, G. N., Kirkpatrick, J. D., Cushing, M. C., et al. 2013, ApJS, 205, 6
Madsen, S., Dravins, D., & Lindegren, L. 2002, A&A, 381, 446
Magnier, E. A., Schlafly, E. F., Finkbeiner, D. P., et al. 2020, ApJS, 251, 6
Mamajek, E. E. 2007, in IAU Symp. 237, Triggered Star Formation in a Turbulent ISM, ed. B. G. Elmegreen & J. Palous (Cambridge: Cambridge Univ. Press), 442
Manjavacas, E., Goldman, B., Reffert, S., et al. 2013, A&A, 560, A52
Marocco, F., Day-Jones, A. C., Lucas, P. W., et al. 2014, MNRAS, 439, 372
Marocco, F., Eisenhardt, P. R. M., Fowler, J. W., et al. 2021, ApJS, 253, 8
Marocco, F., Jones, H. R. A., Day-Jones, A. C., et al. 2015, MNRAS, 449, 3651
Marocco, F., Smart, R. L., Mamajek, E. E., et al. 2020, MNRAS, 494, 4891
Martin, E. C., Kirkpatrick, J. D., Beichman, C. A., et al. 2018, ApJ, 867, 109
Martín, E. L., Lodieu, N., & Béjar, V. J. S. 2020, A&A, 640, A9
McMahon, R. G., Banerji, M., Gonzalez, E., et al. 2013, Msngr, 154, 35
Meisner, A. M., Caselden, D., Kirkpatrick, J. D., et al. 2020a, ApJ, 889, 74
Meisner, A. M., Faherty, J. K., Kirkpatrick, J. D., et al. 2020b, ApJ, 899, 123
Meisner, A. M., Schneider, A. C., Burgasser, A. J., et al. 2021, ApJ, 915, 120
Metchev, S. A., Kirkpatrick, J. D., Berriman, G. B., et al. 2008, ApJ, 676, 1281

Mugrauer, M., Seifahrt, A., Neuhäuser, R., et al. 2006, MNRAS, 373, L31
Mužić, K., Radigan, J., Jayawardhana, R., et al. 2012, AJ, 144, 180
Naud, M.-E., Artigau, É., Malo, L., et al. 2014, ApJ, 787, 5
Nissen, P. E. 2004, in Origin and Evolution of the Elements, ed. A. McWilliam & R. Michael (Cambridge: Cambridge Univ. Press), 154
Pérez-Garrido, A., Lodieu, N., & Rebolo, R. 2017, A&A, 599, A78
Pérez-Garrido, A., Lodieu, N., Rebolo, R., et al. 2018, A&A, 620, A130
Pickles, A., & Depagne, É. 2010, PASP, 122, 1437
Pineda, J. S., Hallinan, G., Kirkpatrick, J. D., et al. 2016, ApJ, 826, 73
Radigan, J., Jayawardhana, R., Lafrenière, D., et al. 2013, ApJ, 778, 36
Radigan, J., Lafrenière, D., Jayawardhana, R., et al. 2008, ApJ, 689, 471
Rebolo, R., Zapatero Osorio, M. R., Madruga, S., et al. 1998, Sci, 282, 1309
Reid, I. N., Cruz, K. L., Kirkpatrick, J. D., et al. 2008, AJ, 136, 1290
Reid, I. N., Gizis, J. E., Kirkpatrick, J. D., et al. 2001, AJ, 121, 489
Reid, I. N., Kirkpatrick, J. D., Gizis, J. E., et al. 2000, AJ, 119, 369
Reid, I. N., Lewitus, E., Allen, P. R., et al. 2006, AJ, 132, 891
Reylé, C. 2018, A&A, 619, L8
Reylé, C., Delorme, P., Willott, C. J., et al. 2010, A&A, 522, A112
Riedel, A. R., Blunt, S. C., Lambrides, E. L., et al. 2017, AJ, 153, 95
Riedel, A. R., DiTomasso, V., Rice, E. L., et al. 2019, AJ, 157, 247
Robert, J., Gagné, J., Artigau, É., et al. 2016, ApJ, 830, 144
Sahlmann, J., Burgasser, A. J., Bardalez Gagliuffi, D. C., et al. 2020, MNRAS, 495, 1136
Sahlmann, J., Lazorenko, P. F., Bouy, H., et al. 2016, MNRAS, 455, 357
Sapozhnikov, S., & Kovaleva, D. 2021, OAst, 30, 191
Schaefer, G. H., White, R. J., Baines, E. K., et al. 2018, ApJ, 858, 71
Schilbach, E., Röser, S., & Scholz, R.-D. 2009, A&A, 493, L27
Schmidt, S. J., Cruz, K. L., Bongiorno, B. J., et al. 2007, AJ, 133, 2258
Schmidt, S. J., Hawley, S. L., West, A. A., et al. 2015, AJ, 149, 158
Schmidt, S. J., West, A. A., Hawley, S. L., et al. 2010, AJ, 139, 1808
Schneider, A. C., Burgasser, A. J., Bruursema, J., et al. 2023, ApJL, 943, L16
Schneider, A. C., Burgasser, A. J., Gerasimov, R., et al. 2020, ApJ, 898, 77
Schneider, A. C., Cushing, M. C., Kirkpatrick, J. D., et al. 2014, AJ, 147, 34
Schneider, A. C., Greco, J., Cushing, M. C., et al. 2016, ApJ, 817, 112
Schneider, A. C., Vrba, F. J., Munn, J. A., et al. 2022, AJ, 163, 242
Schneider, A. C., Windsor, J., Cushing, M. C., et al. 2017, AJ, 153, 196
Schneider, D. P., Knapp, G. R., Hawley, S. L., et al. 2002, AJ, 123, 458
Scholz, R.-D. 2010, A&A, 515, A92
Scholz, R.-D. 2020, A&A, 637, A45
Scholz, R.-D., Bihain, G., Schnurr, O., et al. 2011, A&A, 532, L5
Scholz, R.-D., Lodieu, N., & McCaughrean, M. J. 2004, A&A, 428, L25
Scholz, R.-D., Storm, J., Knapp, G. R., et al. 2009, A&A, 494, 949
Sheppard, S. S., & Cushing, M. C. 2009, AJ, 137, 304
Siegler, N., Close, L. M., Burgasser, A. J., et al. 2007, AJ, 133, 2320
Simons, D. A., & Tokunaga, A. 2002, PASP, 114, 169
Singh, K., Rothstein, P., Curtis, J. L., et al. 2021, RNAAS, 5, 84
Skrutskie, M. F., Cutri, R. M., Stiening, R., et al. 2006, AJ, 131, 1163
Skrzypek, N., Warren, S. J., & Faherty, J. K. 2016, A&A, 589, A49
Smart, R. L., Marocco, F., Sarro, L. M., et al. 2019, MNRAS, 485, 4423

Smart, R. L., Tinney, C. G., Bucciarelli, B., et al. 2013, MNRAS, 433, 2054
Smith, L., Lucas, P. W., Burningham, B., et al. 2014, MNRAS, 437, 3603
Softich, E., Schneider, A. C., Patience, J., et al. 2022, ApJL, 926, L12
Stern, D., Kirkpatrick, J. D., Allen, L. E., et al. 2007, ApJ, 663, 677
Strauss, M. A., Fan, X., Gunn, J. E., et al. 1999, ApJL, 522, L61
Stumpf, M. B., Brandner, W., Bouy, H., et al. 2010, A&A, 516, A37
Tang, S.-Y., Chen, W. P., Chiang, P. S., et al. 2018, ApJ, 862, 106
Tang, S.-Y., Pang, X., Yuan, Z., et al. 2019, ApJ, 877, 12
Tannock, M. E., Metchev, S., Heinze, A., et al. 2021, AJ, 161, 224
Thompson, M. A., Kirkpatrick, J. D., Mace, G. N., et al. 2013, PASP, 125, 809
Thorstensen, J. R., & Kirkpatrick, J. D. 2003, PASP, 115, 1207
Tinney, C. G. 1993, ApJ, 414, 279
Tinney, C. G., Burgasser, A. J., & Kirkpatrick, J. D. 2003, AJ, 126, 975
Torres, C. A. O., Quast, G. R., Melo, C. H. F., et al. 2008, in Handbook of Star Forming Regions, Vol. II: The Southern Sky ASP Monograph Publications, ed. B. Reipurth, Vol. 5 (San Francisco, CA: ASP), 757
Torres, S., Cantero, C., Rebassa-Mansergas, A., et al. 2019, MNRAS, 485, 5573
Ujjwal, K., Kartha, S. S., Mathew, B., et al. 2020, AJ, 159, 166
van Leeuwen, F. 2007, A&A, 474, 653
Vos, J. M., Allers, K. N., & Biller, B. A. 2017, ApJ, 842, 78
Vos, J. M., Allers, K. N., Biller, B. A., et al. 2018, MNRAS, 474, 1041
Vos, J. M., Biller, B. A., Bonavita, M., et al. 2019, MNRAS, 483, 480
Vos, J. M., Faherty, J. K., Gagné, J., et al. 2022, ApJ, 924, 68
Vrba, F. J., Henden, A. A., Luginbuhl, C. B., et al. 2004, AJ, 127, 2948
West, A. A., Hawley, S. L., Bochanski, J. J., et al. 2008, AJ, 135, 785
West, A. A., Morgan, D. P., Bochanski, J. J., et al. 2011, AJ, 141, 97
Wilson, J. C., Kirkpatrick, J. D., Gizis, J. E., et al. 2001, AJ, 122, 1989
Wilson, J. C., Miller, N. A., Gizis, J. E., et al. 2003, in IAU Symp. 211, Brown Dwarfs, ed. E. Martín (San Francisco, CA: ASP), 197
Wright, E. L., Eisenhardt, P. R. M., Mainzer, A. K., et al. 2010, AJ, 140, 1868
Wright, E. L., Skrutskie, M. F., Kirkpatrick, J. D., et al. 2013, AJ, 145, 84
York, D. G., Adelman, J., Anderson, J. E., et al. 2000, AJ, 120, 1579
Zapatero Osorio, M. R., Béjar, V. J. S., Miles-Páez, P. A., et al. 2014, A&A, 568, A6
Zhang, Z., Liu, M. C., Best, W. M. J., et al. 2021, ApJ, 911, 7
Zhang, Z., Liu, M. C., Hermes, J. J., et al. 2020, ApJ, 891, 171
Zhang, Z. H., Burgasser, A. J., Gálvez-Ortiz, M. C., et al. 2019, MNRAS, 486, 1260
Zhang, Z. H., Pinfield, D. J., Day-Jones, A. C., et al. 2010, MNRAS, 404, 1817
Zhang, Z. H., Pinfield, D. J., Gálvez-Ortiz, M. C., et al. 2017, MNRAS, 464, 3040
Zhang, Z. H., Pokorny, R. S., Jones, H. R. A., et al. 2009, A&A, 497, 619
Zuckerman, B. 2019, ApJ, 870, 27
Zuckerman, B., Bessell, M. S., Song, I., et al. 2006, ApJL, 649, L115
Zuckerman, B., Song, I., & Bessell, M. S. 2004, ApJL, 613, L65
Zuckerman, B., Song, I., Bessell, M. S., et al. 2001, ApJL, 562, L87